Sox5–/–;Sox6–/– mice died in utero with virtual absence of cartilage [26]. In these mice, mesenchymal condensations were formed, but there was no overt chondrocyte differentiation. Expression of chondrocyte marker genes was severely reduced, while levels of Sox9 mRNA were comparable to those in wild-type cartilage. Inactivation of the *Sox9* gene in limb buds using the Cre recombinase/loxP recombination system before chondrogenic mesenchymal condensations resulted in loss of Sox5 and Sox6 expression. Inactivation of the *Sox9* gene using the Cre recombinase/loxP recombination system after chondrogenic mesenchymal condensations caused severe generalized chondrodysplasia similar to that seen in *Sox5–/–;Sox6–/–* mice. These data demonstrate important and redundant roles of Sox5 and Sox6 that lie downstream of Sox9 in chondrogenic differentiation after mesenchymal condensations (Fig. 1).

Roles of the combination of Sox5, Sox6, and Sox9 in chondrogenic differentiation

By utilizing the differentiation and proliferation capabilities of stem cells, regenerative medicine attempts to treat irreversible organ failures that cannot be dealt with by the conventional medical treatment. In the skeletal area, cartilage has a relatively poor regenerative capacity, and thus may benefit most from regenerative medicine. Conditions such as osteoarthritis and congenital skeletal defects are apparent targets with great medical and socioeconomic impacts. To make cartilage regenerative medicine a reality, it is important to know the sufficient conditions for chondrogenic differentiation. Although the above-mentioned lines of evidence demonstrate that Sox5, Sox6, and Sox9 are necessary for chondrogenic differentiation at different steps, the question remains whether they constitute a signal sufficient to activate the process.

To screen for the sufficient conditions for chondrogenic differentiation, we needed a monitoring system that could detect chondrogenic differentiation in an easy, precise, and noninvasive fashion. For this purpose, we established transgenic mice expressing a chondrocyte-specific Col2a1 promoter–green fluorescent protein (GFP) reporter gene and isolated totipotent, undifferentiated ES cells from them (Col2-GFP ES) [27]. Since GFP expression was specifically localized in cartilage in these mice, ES cells from these mice were expected to fluoresce solely upon chondrogenic differentiation. Using this system, we examined the effects of gain- and loss-of-function of representative factors that are known to be important for this differentiation: Sox5, Sox6, Sox9, IGF-1, FGF2, Ihh, BMP2, TGF-β, and Wnts. Because we intended to find factors affecting chondrogenic differentiation directly rather than indirectly, the assessment of fluorescence was done within 3 days after transduction. The result was that no single factor caused fluorescence; hence, we screened for all possible combinations of these factors. It turned out that GFP expression was observed only upon treatment with the combination of Sox5, 6, and 9 (the Sox trio), while there was no fluorescence upon treatment with

other combinations that included each Sox alone within this period (data not shown). When expression levels of the chondrocyte marker genes were analyzed, the Sox trio combination successfully induced them. Similar results were obtained in human mesenchymal stem cells (hMSC) and even in nonchondrogenic human immortalized cell lines (HeLa derived from the cervix, HuH-7 from the liver, and HEK293 from the kidney) and human dermal fibroblasts (hDF).

We next examined the effect of different culture systems on chondrogenic differentiation induced by the Sox trio. Three-dimensional (3D) cell–cell interactions as well as extracellular matrix are known to influence differentiation potentials of many cell types. A monolayer culture has been reported to be disadvantageous to chondrogenic differentiation, so spheroid and 3D cultures have been preferably performed. If the Sox trio provided signals sufficient for chondrogenic differentiation, it might obviate the use of these specific culture formats. To test this possibility, we compared expression levels of the cartilage marker genes by hMSC and hDF cultured in a monolayer, in spheroids, or in 3D collagen. These genes were upregulated efficiently regardless of the culture system.

Sox9 has been shown to be necessary for the expression of Sox5 and Sox6 [17], and, therefore, Sox9 might induce expression of Sox5 and Sox6, but the hypothesis has never been proven directly. In our experiments, hMSC treated with Sox9 alone and cultured for 1 week started expressing Sox5 and Sox6 mRNAs, whereas those treated with LacZ did not. Similar results were obtained with ES cells and hDF. In contrast to the conventional chondrogenic techniques, the combination of the three Sox genes suppressed hypertrophic and osteogenic differentiation (Fig. 1).

Lastly, to test whether the Sox trio could influence cartilage formation in vivo, we directly introduced the Sox trio genes into the subcutaneous tissue. Adenoviruses expressing the Sox trio were injected into the subcutaneous tissue in front of the mouse tibia, and the mice were sacrificed 1 week after the treatment and analyzed by histology and immunohistochemistry. Chondrocyte-like cells appeared in the area adjacent to the bone, and they stained positive for Safranin-O and type II collagen immunoreactivity.

Summary

Sox9 is necessary for chondrogenic differentiation both before and after mesenchymal condensations, while Sox5 and Sox6 are necessary only after mesenchymal condensations. However, no individual Sox is sufficient for the process, since none individually induced the differentiation in various cell types, including ES cells, nonchondrogenic immortalized cells, and nonchondrogenic adult cells. Only when Sox5, Sox6, and Sox9 were combined was the differentiation successfully induced in all cell types and also in vivo, suggesting that the combination provides signals sufficient for the differentiation [27]. The potent in vitro chondrogenic system via the combination of the three Sox genes not

only provides a new in vitro chondrogenic differentiation model, which may help us better understand the mechanism of this process, but also adds a powerful tool to cartilage regenerative medicine.

References

1. Karaplis AC (2002) Embryonic development of bone and the molecular regulation of intramembranous and endochondral bone formation. In: Bilezikian JP, Raisz LG, Rodan GA (eds) Principles of Bone Biology, 2nd ed., vol. 1. Academic, San Diego, pp 33–58
2. Johnson RL, Tabin CJ (1997) Molecular models for vertebrate limb development. Cell 90:979–990
3. Hall BK, Miyake T (2000) All for one and one for all: condensations and the initiation of skeletal development. Bioessays 22:138–147
4. Kronenberg HM (2003) Developmental regulation of the growth plate. Nature 423:332–336
5. Chung UI, Schipani E, McMahon AP, Kronenberg HM (2001) Indian hedgehog couples chondrogenesis to osteogenesis in endochondral bone development. J Clin Invest 107:295–304
6. Long F, Chung U, Ohba S, McMahon J, Kronenberg H, McMahon AP (2004) Genetic evidence that Ihh signaling is directly required for the osteoblast lineage in the endochondral skeleton. Development 131:1309–1318
7. de Crombrugghe B, Lefebvre V, Nakashima K (2001) Regulatory mechanisms in the pathways of cartilage and bone formation. Curr Opin Cell Biol 13:721–727
8. Wegner M (1999) From head to toes: the multiple facets of Sox proteins. Nucleic Acids Res 27:1409–1420
9. Lefebvre V, Huang W, Harley VR, Goodfellow PN, de Crombrugghe B (1997) SOX9 is a potent activator of the chondrocyte-specific enhancer of the pro alpha1(II) collagen gene. Mol Cell Biol 17:2336–2346
10. Ng LJ, Wheatley S, Muscat GE, Conway-Campbell J, Bowles J, Wright E, Bell DM, Tam PP, Cheah KS, Koopman P (1997) SOX9 binds DNA, activates transcription, and coexpresses with type II collagen during chondrogenesis in the mouse. Dev Biol 183:108–121
11. Wright E, Hargrave MR, Christiansen J, Cooper L, Kun J, Evans T, Gangadharan U, Greenfield A, Koopman P (1995) The Sry-related gene *Sox9* is expressed during chondrogenesis in mouse embryos. Nat Genet 9:15–20
12. Zhao Q, Eberspaecher H, Lefebvre V, De Crombrugghe B (1997) Parallel expression of Sox9 and Col2a1 in cells undergoing chondrogenesis. Dev Dyn 209:377–386
13. Foster JW, Dominguez-Steglich MA, Guioli S, Kowk G, Weller PA, et al. (1994) Campomelic dysplasia and autosomal sex reversal caused by mutations in an SRY-related gene. Nature 372:525–530
14. Wagner T, Wirth J, Meyer J, Zabel B, Held M, et al. (1994) Autosomal sex reversal and campomelic dysplasia are caused by mutations in and around the SRY-related gene *SOX9*. Cell 79:1111–1120
15. Bi W, Huang W, Whitworth DJ, Deng JM, Zhang Z, Behringer RR, de Crombrugghe B (2001) Haploinsufficiency of Sox9 results in defective cartilage primordia and premature skeletal mineralization. Proc Natl Acad Sci U S A 98:6698–6703
16. Bi W, Deng JM, Zhang Z, Behringer RR, de Crombrugghe B (1999) Sox9 is required for cartilage formation. Nat Genet 22:85–89
17. Akiyama H, Chaboissier MC, Martin JF, Schedl A, de Crombrugghe B (2002) The transcription factor Sox9 has essential roles in successive steps of the chondrocyte differentiation pathway and is required for expression of Sox5 and Sox6. Genes Dev 16:2813–2828
18. Bridgewater LC, Lefebvre V, de Crombrugghe B (1998) Chondrocyte-specific enhancer elements in the *Col11a2* gene resemble the Col2a1 tissue-specific enhancer. J Biol Chem 273:14998–15006
19. Xie WF, Zhang X, Sakano S, Lefebvre V, Sandell LJ (1999) Transactivation of the mouse cartilage-derived retinoic acid-sensitive protein gene by Sox9. J Bone Miner Res 14:757–763
20. Bell DM, Leung KK, Wheatley SC, Ng LJ, Zhou S, Ling KW, Sham MH, Koopman P, Tam PP, Cheah KS (1997) SOX9 directly regulates the type-II collagen gene. Nat Genet 16:174–178
21. Ambrosetti DC, Basilico C, Dailey L (1997) Synergistic activation of the fibroblast growth factor 4 enhancer by Sox2 and Oct-3 depends on protein–protein interactions facilitated by a specific spatial arrangement of factor binding sites. Mol Cell Biol 17:6321–6329
22. Kamachi Y, Cheah KS, Kondoh H (1999) Mechanism of regulatory target selection by the SOX high-mobility-group domain proteins as revealed by comparison of SOX1/2/3 and SOX9. Mol Cell Biol 19:107–120
23. Kamachi Y, Uchikawa M, Kondoh H (2000) Pairing SOX off: with partners in the regulation of embryonic development. Trends Genet 16:182–187
24. Lefebvre V, de Crombrugghe B (1998) Toward understanding SOX9 function in chondrocyte differentiation. Matrix Biol 16:529–540
25. Denny P, Swift S, Connor F, Ashworth A (1992) An SRY-related gene expressed during spermatogenesis in the mouse encodes a sequence-specific DNA-binding protein. EMBO J 11:3705–3712
26. Smits P, Li P, Mandel J, Zhang Z, Deng JM, Behringer RR, de Croumbrugghe B, Lefebvre V (2001) The transcription factors L-Sox5 and Sox6 are essential for cartilage formation. Dev Cell 1:277–290
27. Ikeda T, Kamekura S, Mabuchi A, Kou I, Seki S, Takato T, Nakamura K, Kawaguchi H, Ikegawa S, Chung UI (2004) The combination of SOX5, SOX6, and SOX9 (the SOX trio) provides signals sufficient for induction of permanent cartilage. Arthritis Rheum 50:3561–3573

Involvement of Endogenous Bone Morphogenetic Protein (BMP) 2 and BMP6 in Bone Formation*

Fumitaka Kugimiya[‡§], Hiroshi Kawaguchi[§], Satoru Kamekura[§], Hirotaka Chikuda[§], Shinsuke Ohba[‡], Fumiko Yano[‡], Naoshi Ogata[‡], Takenobu Katagiri[¶], Yoshifumi Harada[∥], Yoshiaki Azuma[∥], Kozo Nakamura[§], and Ung-il Chung[‡1]

From the Divisions of [‡]Tissue Engineering and [§]Sensory & Motor System Medicine, Faculty of Medicine, University of Tokyo, Hongo 7-3-1, Bunkyo, Tokyo, 113-8655, the [¶]Division of Pathophysiology, Research Center for Genomic Medicine, Saitama Medical School, Yamane 1397-1, Hidaka, Saitama, 350-1241, and [∥]Teijin Co., Ltd., Asahigaoka 4-3-2, Hino, Tokyo 191-8512, Japan

Although accumulated evidence has shown the bone anabolic effects of bone morphogenetic proteins (BMPs) that were exogenously applied *in vitro* and *in vivo*, the roles of endogenous BMPs during bone formation remain to be clarified. This study initially investigated expression patterns of BMPs in the mouse long bone and found that BMP2 and BMP6 were the main subtypes expressed in hypertrophic chondrocytes that induce endochondral bone formation. We then examined the involvement of the combination of these BMPs in bone formation *in vivo* by generating the compound-deficient mice (*Bmp2+/−;Bmp6−/−*). Under physiological conditions, these mice exhibited moderate growth retardation compared with the wild-type (WT) littermates during the observation period up to 52 weeks of age. Both the fetal and adult compound-deficient mice showed a reduction in the trabecular bone volume with suppressed bone formation, but normal bone resorption, whereas the single deficient mice (*Bmp2+/−* or *Bmp6−/−*) did not. When a fracture was created at the femoral midshaft and the bone healing was analyzed, the endochondral bone formation, but not intramembranous bone formation, was impaired by the compound deficiency. In the cultures of bone marrow cells, however, there was no difference in osteogenic differentiation between WT and compound-deficient cells in the presence or absence of the exogenous BMP2. We thus concluded that endogenous BMP2 and BMP6 cooperatively play pivotal roles in bone formation under both physiological and pathological conditions.

Bone morphogenetic proteins (BMPs)[2] are members of secreted signaling proteins that belong to the transforming growth factor-β superfamily. BMPs were originally identified as molecules that induced ectopic bone formation when implanted into rodent muscles (1, 2). In accordance with such *in vivo* effects, BMPs have been shown to regulate osteogenic differentiation *in vitro* (3). However, naturally occurring or genetically engineered mice deficient in BMPs reported so far are either normal, exhibit abnormalities in skeletal patterning, or die during early embryonic development, thus being non-informative as to the role of endogenous BMPs in bone formation (4, 5).

In mammals, there are two distinct modes of bone formation: intramembranous and endochondral (6). Most of the bones form through the latter process, which is characterized by the replacement of a cartilage mold by bone and bone marrow (7). During this process, cells in the mesenchymal condensations become chondrocytes, the primary cell type of cartilage; cells at the border of the condensations form a perichondrium. Chondrocytes have a characteristic shape, express a characteristic genetic program driven by SOX9 and other transcription factors, and secrete a matrix rich in type II collagen and proteoglycan. Cartilage enlarges through chondrocyte proliferation and matrix production. Chondrocytes in the center of the cartilage mold then stop proliferating, enlarge (hypertrophy), and change their genetic program to synthesize the type X collagen. Hypertrophic chondrocytes mineralize their surrounding matrix, attract blood vessels through the production of the vascular endothelial growth factor and other factors, and attract chondroclasts and osteoclasts. Moreover, these chondrocytes direct mesenchymal cells in the perichondrium and in the bone marrow to become osteoblasts, which form the bone collar and the primary spongiosa (8, 9). Thus, during the endochondral bone formation, hypertrophic chondrocytes link chondrogenesis to osteogenesis by inducing osteogenesis and angiogenesis (8, 9). Hypertrophic chondrocytes express a number of growth factors, cytokines, and matrix proteins. Among them, Indian hedgehog (Ihh) has been proven to be indispensable for the induction of osteogenesis by these chondrocytes (8, 10). Ihh alone, however, cannot induce bone formation (11), suggesting that other factors secreted from these chondrocytes may also be necessary for osteogenesis. Because some BMPs can induce ectopic bone formation when implanted into rodent muscles and promote osteogenic differentiation *in vitro*, they are strong candidates for the osteogenic factors secreted by these chondrocytes. Among them, BMP2 and BMP6 are known to be expressed by these chondrocytes (8). As is the case with the other BMPs, however, there is no direct evidence that the endogenous BMP2 and BMP6 are involved in bone formation, because homozygous *Bmp2*-deficient (*Bmp2−/−*) mice die during the early embryonic stage (12), and homozygous *Bmp6*-deficient (*Bmp6−/−*) mice show no skeletal abnormality except for a slight delay in the ossification of the sternum (13). We hypothesized that there might be a genetic redundancy between BMP2 and BMP6 in the regulation of bone formation. Hence, the present study generated compound knock-out mice lacking one allele of the *Bmp2* gene and both alleles of the *Bmp6* gene (*Bmp2+/−; Bmp6−/−*) and investigated the effect of their compound loss on bone metabolism under both physiological and pathological conditions.

EXPERIMENTAL PROCEDURES

Animals—Bmp2+/− mice were kindly provided by A. Bradley (Baylor College of Medicine, Houston, TX) (12); *Bmp6−/−* mice by E. Robertson (Harvard University, Cambridge, MA) (13). The mice were maintained in a C57BL/6 background. To generate *Bmp2+/−;*

[1] To whom correspondence should be addressed. Tel.: 81-3-3815-5411 (ext. 37014 or 33376); Fax: 81-3-3818-4082; E-mail: uichung-tky@umin.ac.jp.

[2] The abbreviations used are: BMP, bone morphogenetic protein; Ihh, Indian hedgehog; WT, wild type; RT, reverse transcriptase; BMD, bone mineral density; rh, recombinant human; ALP, alkaline phosphatase; CFU, colony forming unit; MMP-13, metalloproteinase 13.

Bmp6−/− mice, *Bmp2+/−* mice were mated with the homozygous *Bmp6−/−* mice to obtain *Bmp2+/−;Bmp6+/−* mice. *Bmp2+/−; Bmp6+/−* mice were then mated with each other. Because *Bmp2−/−* mice were embryonically lethal, two of 12 live mice were expected to be *Bmp2+/−;Bmp6−/−*. All experiments were performed on male mice in accordance with the protocol approved by the Animal Care and Use Committee of the University of Tokyo.

Genotyping—Genomic DNA was isolated from the tail. 10 ng of genomic DNA was used for genotyping by PCR. The PCR primers were as follows: 5′-AGCATGAACCCTCATGTGTTGG-3′ (forward primer for *Bmp2* wild-type (WT) and mutant alleles), 5′-GTGACATTAG-GCTGCTGTAGCA-3′ (reverse primer for *Bmp2* WT allele), 5′-GAGACTAGTGAGACGTGCTACT-3′ (reverse primer for *Bmp2* mutant allele), 5′-TCCCCACATCAACGACAC-3′ (forward primer for *Bmp6* WT and mutant alleles), 5′-TCCCCACCACACAGTC-CTTG-3′ (reverse primer for *Bmp6* WT allele) and 5′-CGCTGA-CAGCCGGAACACGG-3′ (reverse primer *Bmp6* mutant allele). PCR were performed at 94 °C for 1 min, at 58 °C for 1 min, and at 72 °C for 1 min for 35 cycles. The PCR product from the WT *Bmp2* allele was 322 bp and that from the *Bmp2* mutant allele, 367 bp. The PCR product from the WT *Bmp6* allele was 112 bp and that from the *Bmp6* mutant allele, 499 bp.

Skeletal Preparation—Embryos at E17.5 were eviscerated, fixed in 100% ethanol for 4 days, and then transferred to 100% acetone. After 3 days, they were rinsed with water and stained for 10 days in staining solution containing 1 volume of 0.1% Alizarin red S (Sigma), 95% ethanol; 1 volume of 0.3% Alcian blue 8GX (Sigma), 70% ethanol; 1 volume of 100% acetic acid, and 17 volumes of 100% ethanol. After rinsing with 96% ethanol, the specimens were kept in 20% glycerol, 1% KOH at 37 °C for 16 h and subsequently at room temperature until the skeletons became clearly visible. For storage, the specimens were transferred to 50, 80, and finally 100% glycerol (14).

Histological Analysis—For the histological analysis, embryonic limbs were fixed in 4% paraformaldehyde/phosphate-buffered saline for 1 h and embedded in paraffin for sectioning, according to the standard procedures. Sections (5 μm thick) were then stained with Hematoxylin and Eosin (H&E) for morphological study, with toluidine blue for detection of the cartilage matrix, or with 5% silver nitrate for detection of mineralization (the von Kossa method), then mounted in xylene-based media, and photographed. For immunohistochemistry, after treatment with 25 μg/ml hyaluronidase for 1 h at 37 °C, the sections were incubated with monoclonal rat anti-mouse antibodies against the type I, II, and X collagens (LSL, Tokyo, Japan), and MMP-13 (CHEMICON International, Inc., Temecula, CA) for 12–24 h at 4 °C. To visualize the immunoreactivity for type I, II, and X collagens using fluorescence, the sections were incubated with the Alexa 488 anti-rabbit IgG antibody (Molecular Probes) for 1 h at room temperature. To visualize the immunoreactivity for MMP-13, the sections were incubated with the horseradish peroxidase-conjugated goat antibodies against rabbit IgG (ICN Biomedicals, Inc., Aurora, OH) for 20 min at room temperature, immersed in a diaminobenzidine solution for 10 min at room temperature, then counterstained with methylgreen. As a control, rabbit nonimmune serum (Upstate Biotechnology, Charlottesville, VA) was used at the same dilution instead of the primary antibody. To quantify the areas of interest, NIH Image was used to measure the ratio to the total area.

In Situ Hybridization—Tissues were fixed in 4% paraformaldehyde/ phosphate-buffered saline overnight at 4 °C, processed, embedded in paraffin, and cut. The *in situ* hybridization was performed as previously described (15) using complementary ^{35}S-labeled riboprobes for mouse

BMP2, BMP4, BMP6, BMP7, GDF5 (kindly provided by E. Robertson, Harvard University) (13), and type I collagen (8).

Real-time RT-PCR—Total RNA was extracted using an ISOGEN Kit (Wako Pure Chemicals Industry, Ltd., Tokyo) and an RNeasy Mini Kit (Qiagen, Hilden, Germany), then treated with DNase I (Qiagen), according to the manufacturer's instructions. One μg of RNA was reverse transcribed using a Takara RNA PCR Kit (AMV) version 2.1 (Takara Shuzo Co., Shiga, Japan) to generate the single-stranded cDNA. PCR was performed with the ABI Prism 7000 Sequence Detection System (Applied Biosystems, Foster City, CA). Each PCR consisted of 1× QuantiTect SYBR Green PCR Master Mix (Qiagen), 0.3 μM specific primers, and 500 ng of cDNA. The mRNA copy number of a specific gene in the total RNA was calculated with a standard curve generated using serially diluted plasmids containing PCR amplicon sequences and normalized to the human or rodent total RNA (Applied Biosystems) with mouse actin as the internal control. Standard plasmids were synthesized using a TOPO TA Cloning Kit (Invitrogen, Carlsbad, CA), according to the manufacturer's instructions. All reactions were run in triplicate. The primer sequences are available upon request.

Radiological Analysis—Bone radiographs were taken with a soft x-ray instrument (CMB-2, SOFTEX, Kanagawa, Japan). A three-dimensional CT scan was taken with a composite x-ray analyzing system (NX-HCP, NS-ELEX Inc., Tokyo). The bone mineral density (BMD) was measured by single energy x-ray absorptiometry using a bone mineral analyzer (DCS-600R, Aloka Co., Tokyo).

Bone Histomorphometry—Eight 9-week-old mice were used in each group. For Villanueva-Goldner staining, tibias were fixed with ethanol, embedded in methyl methacrylate, and sectioned in 6-μm slices. For double labeling, the mice were subcutaneously injected with 8 mg/kg body weight of calcein at 3 and 10 days before sacrifice. Tartrate-resistand acid phosphatase-positive cells were stained at pH 5.0 in the presence of L-(+)-tartaric acid with naphthol AS-MX phosphate (Sigma) in *N,N*-dimethyl formamide as the substrate. The specimens were subjected to histomorphometric analyses using an image analyzer (Histometry RT CAMERA, System Supply Co., Nagano, Japan). The parameters of the trabecular bone were measured in an area 1.2 mm in length from 0.5 mm below the growth plate at the proximal metaphysis of the tibias. The parameters of the cortical bone were measured at the midshaft of the tibias. The thickness of the growth plate was measured at the proximal tibias.

Fracture Model—Bone fractures were generated as previously described (16). Eight 9-week-old mice were used in each group. Briefly, under general anesthesia with xylazine (0.05 mg/10 g body weight) and ketamine (0.5 mg/10 g body weight, Sigma), a 15-mm incision was longitudinally made to expose the femur. A transverse osteotomy was performed with a bone saw (Volvere GX, NSK Nakanishi, Inc., Tochigi, Japan) at the middle of the femur. Fractured bones were repositioned, and then the full-length of the bone marrow cavity was internally stabilized with an intramedullary nail with the inner pin of a 23-gauge spinal needle. The animals were allowed activity, diet, and water *ad libitum*. For the histological analyses, the animals were killed at 5, 7, and 18 days after surgery by asphyxiation with carbon dioxide, and their femurs were excised. The calcified area and the bone mineral content of the entire femur were measured. The % gain of calcified area and the % gain of BMC were calculated, and the differences were compared between WT, *Bmp2+/−*, *Bmp6−/−*, and *Bmp2+/−;Bmp6−/−* mice. To distinguish between the intramembranous bone formation and endochondral bone formation during fracture healing, the callus was divided into three equal portions along the axis of the bone. The distal and proximal portions, where bones mainly form through the intramembranous

process (17), were designated as the peripheral part, and the middle portion, where bones mainly form through the endochondral process (17), was designated as the central part. In each part, we measured the ratio of the calcified area to the total area of the histological sections using NIH Image.

Serum and Urinary Biochemistry—Blood samples from 9-week-old WT and *Bmp2+/−;Bmp6−/−* mice (n = 6 for each group) were collected by heart puncture under anesthesia with nembutal (0.4 mg/10 g body weight) (Dainippon Pharmaceutical Co., Ltd., Tokyo). Urine samples were collected for 24 h before sacrifice in oil-sealed bottles in the metabolism cages (CL-0305, CLEA Japan, Inc., Tokyo). The levels of creatinine, calcium, and inorganic phosphorus in the serum were measured using a standard colorimetric technique, a Calcium HR Kit (Wako Pure Chemical Industries, Ltd.), and an Inorganic Phosphorus II Kit (Wako Pure Chemical Industries, Ltd.), respectively, by an autoanalyzer (Type 7170, Hitachi High-Technologies Co., Tokyo). Urinary deoxypyridinoline was measured using a Pyriliks-D enzyme-linked immunosorbent assay kit (Metra Biosystems, Inc., Mountain View, CA). The values were corrected for urinary creatinine measured by a standard colorimetric technique using the Type 7170 autoanalyzer.

In Vitro Bone Marrow Differentiation Assay—Bone marrow cells were isolated from WT and *Bmp2+−;Bmp6−/−* mice at 3 weeks of age and inoculated at a density of 2×10^5 cells/well onto 24-well plates in α-minimal essential medium containing 50 μg/ml ascorbic acid, 10 mM β-glycerophosphate, and ITS+1 liquid media supplement ($\times$100) (Sigma) (osteogenic medium). For treatment with BMP, we added recombinant human (rh) BMP2 at 200 ng/ml. We changed the medium every 4 days with BMP2 being replenished each time. Two weeks after confluence, total RNA was extracted, and alkaline phosphatase (ALP), Alizarin red S, and von Kossa stainings were performed. For ALP staining, cells were fixed in 70% EtOH and stained for 10 min with a solution containing 0.01% naphtol AS-MX phosphate disodium salt (Sigma), 1% *N,N*-dimethyl formamide (Wako Pure Chemicals Industry, Ltd.), and 0.06% fast blue BB (Sigma). For the Alizarin red S staining, the cells were fixed in 10% formalin/phosphate-buffered saline and stained for 10 min with 2% Alizarin red S, pH 4.0, (Sigma) solution. For the von Kossa staining, the cells were fixed with 100% ethanol at room temperature for 15 min, stained with 5% silver nitrate solution (Wako Pure Chemicals Industry, Ltd.) under ultraviolet light for 10 min, and incubated for 5 min with 5% sodium thiosulfate solution (Wako Pure Chemicals Industry, Ltd.).

The numbers of total fibroblastic colonies (CFU-F), ALP positive colonies (CFU-ALP), and bone nodules were assessed as described (18–20). In brief, bone marrow cells isolated from WT and *Bmp2+/−; Bmp6−/−* mice at 3 weeks of age were disseminated into a six-well plate at a concentration of 5×10^5 cells/ml and cultured in osteogenic medium for 5, 10, and 15 days in the presence or absence of rhBMP2 at 200 ng/ml. Subsequently, cells were fixed with 10% neutral-buffered formalin and subjected to the ALP or von Kossa stainings as described above. Colonies consisting of more than 50 cells were defined as CFU-F, and ALP-positive CFU-F were defined as CFU-ALP. Bone nodules were counted on a grid under low power microscopy.

Statistical Analysis—The means of the groups were compared by analysis of variance, and the significance of differences was determined by post-hoc testing using Bonferronis method.

RESULTS

BMP Subtypes Expressed by Hypertrophic Chondrocytes—To determine the BMP subtypes expressed by hypertrophic chondrocytes, we performed *in situ* hybridization for BMPs known to be expressed in chondrocytes (5). Consistent with the previous report (8), the main BMP subtypes expressed by hypertrophic chondrocytes were BMP2 and BMP6 (Fig. 1*A*). As for the other BMPs examined, BMP4 was weakly expressed in the prehypertrophic chondrocytes, BMP7 in the proliferating chondrocytes, and GDF5 in the periarticular proliferating chondrocytes.

Analysis of Fetal Bmp2−/−;Bmp6−/− Mice—To investigate the roles of the enodogenous BMP2 and BMP6 during bone formation, we generated their compound-deficient mice by appropriate mating. Because of the early embryonic lethality of *Bmp2−/−* mice, we studied the bone phenotypes of *Bmp2+/−;Bmp6−/−* mice. To macroscopically visualize bone and cartilage elements, whole embryos at E17.5 were double stained with Alizarin red and Alcian blue (Fig. 1*B*). The staining revealed a normal skeletal patterning in the single deficient (*Bmp2+/−* and *Bmp6−/−*) and the compound-deficient mice. However, the size of the compound-deficient mice was smaller than that of WT mice, whereas that of the single deficient mice was not. Temporal profiles of the body length and weight of the compound-deficient mice showed an ~5% decrease in axial growth and body weight throughout life (Fig. 1*C*).

Histological analysis of the growth plate of the proximal tibias from the E17.5 WT and *Bmp2+/−;Bmp6−/−* mice disclosed that the size of the compound-deficient growth plate was smaller than that of WT (643 $\pm$ 17 *versus* 723 $\pm$ 24 μm, $p < 0.05$), but the proportions of the distinct layers of the growth plate chondrocytes were not significantly different between the two groups (the layer of proliferating chondrocytes, 72.9 $\pm$ 2.3 *versus* 72.1 $\pm$ 2.6%; the layer of hypertrophic chondrocytes, 27.1 $\pm$ 0.8 *versus* 27.9 $\pm$ 0.9%) (Fig. 1*D*). Immunohistochemistry of the type II and X collagens showed no remarkable difference between the two groups (Fig. 1*E*).

To evaluate bone formation in the fetal growth plate, we performed immunohistochemistry and real-time RT-PCR detecting the type I collagen (Fig. 1*F*) and von Kossa staining (Fig. 1*G*). The type I collagen immunoreactivity and type I collagen mRNA expression in the tibia were similar between the compound-deficient and WT mice. The von Kossa staining revealed that the mineralized area in the primary spongiosa of the compound-deficient mice was reduced in comparison with that of WT, although the mineralized area in the hypertrophic layer was similar between the two groups. The number of osteoclasts of the compound-deficient mice was not significantly different from that of WT (data not shown). During endochondral bone formation, osteogenesis is influenced by chondrogenesis. To rule out the possibility that the reduced mineralization of the primary spongiosa of the compound-deficient mice was because of a cartilage defect, we investigated whether chondrocytes reached terminal differentiation by examining the onset of hypertrophic differentiation and cartilage mineralization. H&E staining, immunohistochemical analysis with anti-type X collagen and MMP-13 antibodies, and von Kossa staining of the metatarsal bone sections at E15.5 showed that neither hypertrophic differentiation nor cartilage mineralization occurred in WT or compound-deficient mice (Fig. 1*H*). At E16.5, chondrocytes in the center of the cartilage underwent hypertrophic differentiation, expressing type X collagen and mineralizing the surrounding matrix in both WT and *Bmp2+/−; Bmp6−/−* mice. MMP-13, a marker of terminally differentiated hypertrophic chondrocytes (21–23), just began to be expressed in both groups. At E17.5, MMP-13 expression was markedly up-regulated, the area of the mineralized cartilaginous matrix was increased, and the bone collar was formed in both groups. Thus, no abnormality of terminal differentiation of the chondrocytes was detected in the compound-deficient mice. Taken together, these data suggest that the differentiation/
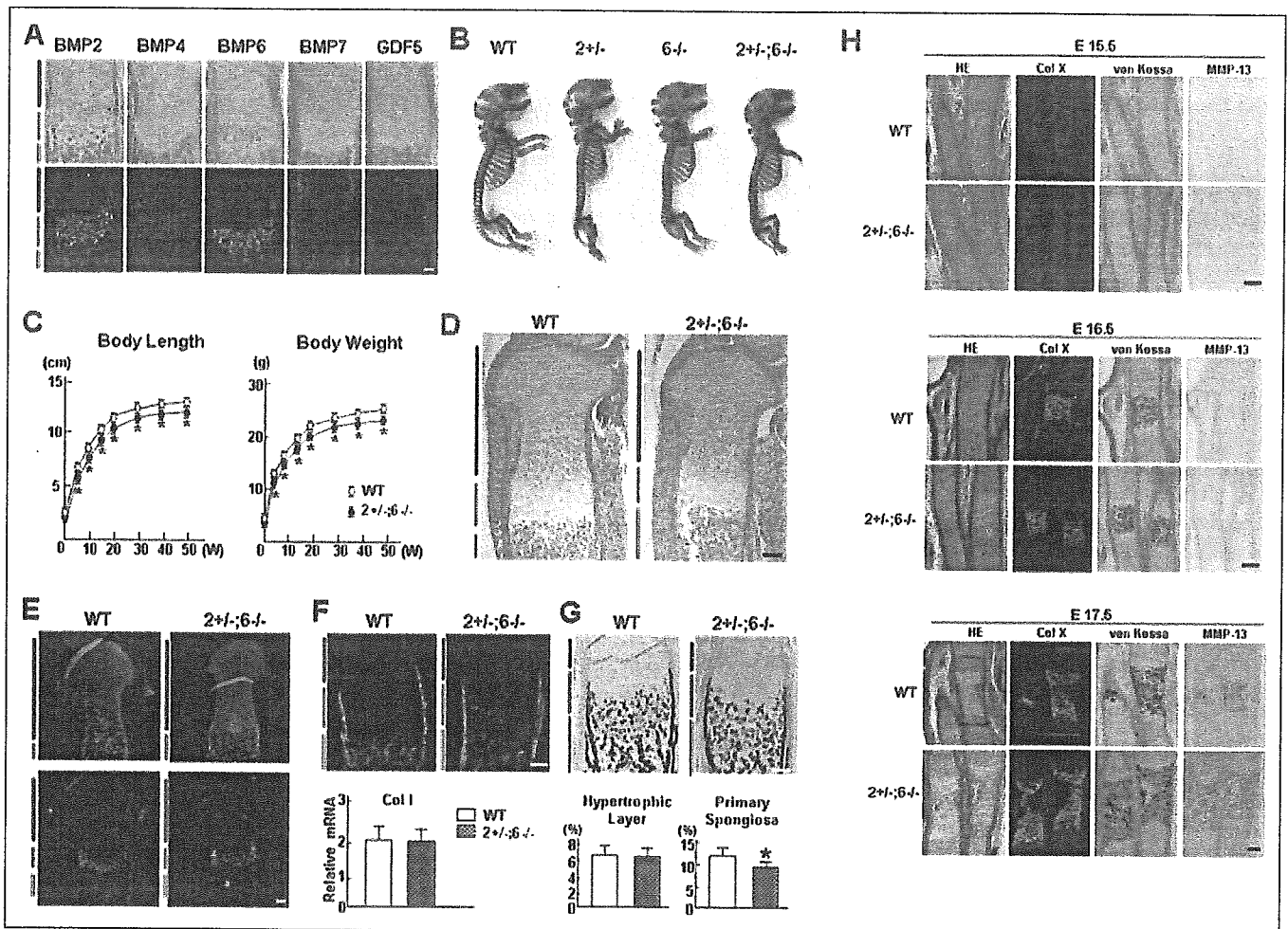
FIGURE 1. **Macroscopic and histological analyses of fetal** *Bmp2+/−;Bmp6−/−* **mice.** *A, in situ* hybridization of the radius growth plates from E17.5 WT mice with mouse BMP2, BMP4, BMP6, BMP7, and GDF5 antisense probes. *Upper panels,* bright field views; *lower panels,* dark field views. *Blue, green,* and *red bars* indicate the layer of proliferating chondrocytes, the layer of hypertrophic chondrocytes, and the primary spongiosa, respectively. *Scale bar,* 100 μm. *B,* double staining with Alizarin red and Alcian blue of the whole body from E17.5 WT, *Bmp2+/−, Bmp6−/−,* and *Bmp2+/−;Bmp6−/−* mice. *C,* temporal growth profiles of WT and *Bmp2+/−;Bmp6−/−* mice at 0, 5, 10, 20, 30, 40, and 50 weeks of age expressed by the body length from nose to tail and body weight. Data are expressed as mean ± S.E. for 12 mice per group. *, *p* < 0.05 *versus* WT. *D,* H&E staining of the tibia sections from E17.5 WT and *Bmp2+/−;Bmp6−/−* mice. *Blue, green,* and *red bars* indicate the layer of proliferating chondrocytes, the layer of hypertrophic chondrocytes, and the primary spongiosa, respectively. *Scale bar,* 100 μm. *E,* immunohistochemical analysis of the tibia sections from E17.5 WT and *Bmp2+/−;Bmp6−/−* mice with anti-type II collagen (*upper panels*) and type X collagen (*lower panels*) antibodies. *Blue, green,* and *red bars* indicate the layer of proliferating chondrocytes, the layer of hypertrophic chondrocytes, and the primary spongiosa, respectively. *Scale bar,* 100 μm. *F,* immunohistochemical analysis with anti-type I collagen antibody of the tibia sections from E17.5 WT and *Bmp2+/−;Bmp6−/−* mice (*upper panels*). Real-time RT-PCR analysis of type I collagen mRNA expression in the tibias from E17.5 WT and *Bmp2+/−;Bmp6−/−* mice (*lower panels*). *Blue, green,* and *red bars* indicate the layer of proliferating chondrocytes, the layer of hypertrophic chondrocytes, and the primary spongiosa, respectively. *Scale bars,* 100 μm. *G,* von Kossa staining of the tibia sections from E17.5 WT and *Bmp2+/−;Bmp6−/−* mice (*upper panels*). The relative ratio of the calcified area in the hypertrophic layer and that in the primary spongiosa were histologically measured (*lower panels*). *Blue, green,* and *red bars* indicate the layer of proliferating chondrocytes, the layer of hypertrophic chondrocytes, and the primary spongiosa, respectively. *Scale bars,* 100 μm. Data are expressed as the mean ± S.E. of 6 mice per genotype. *, *p* < 0.05 *versus* WT. *H,* H&E staining, immunohistochemical analysis with anti-type X collagen and MMP-13 antibodies and von Kossa staining of the metatarsal bone sections at E15.5, E16.5, and E17.5 from WT and *Bmp2+/−;Bmp6−/−* mice. *Scale bar,* 100 μm.

function of osteoblasts is impaired by the compound deficiency of *Bmp2* and *Bmp6*.

Analysis of Adult Bmp2+/−;Bmp6−/− Mice—We then investigated whether the compound deficiency of *Bmp2* and *Bmp6* had effects on the bone metabolism in adult mice. X-rays of the femur at 9 weeks of age showed that the lengths of the femur and the tibia were shorter and that the trabecular bone volume was reduced in *Bmp2+/−;Bmp6+/−* mice compared with that in WT (Fig. 2*A*). Quantitative analysis of the BMD disclosed that the femoral BMD of the compound-deficient mice was reduced compared with that of WT, whereas that of *Bmp2+/−*, *Bmp6+/−, Bmp6−/−,* or *Bmp2+/−;Bmp6+/−* mice was not significantly different from that of WT (Fig. 2*B*). Three-dimensional CT analysis manifested a marked reduction in the trabecular bone volume of the compound-deficient mice (Fig. 2*C*). Next, to investigate the role of endogenous *Bmp2* and *Bmp6* in intramembranous bone formation, the

calvarias were examined. X-ray of the calvarias at 9 weeks of age from WT, *Bmp2+/−, Bmp6−/−,* and *Bmp2+/−;Bmp6−/−* mice did not show any significant difference (Fig. 2*D*), which was confirmed by the quantitative analysis of the BMD (Fig. 2*E*).

Histological analysis with von Kossa staining of the proximal tibia revealed a trabecular bone loss in *Bmp2+/−;Bmp6−/−* mice compared with that in WT (Fig. 3*A*). Although there was no significant difference in the proportions of the growth plates or in the cartilaginous mineralization between the two groups, the mineralization in the primary spongiosa was notably reduced in the compound-deficient mice (Fig. 3*B*). To analyze the mechanism of the bone loss in detail, bone histomorphometric analysis was performed on the tibias (Fig. 3*C*). The bone volume and cortical thickness of the compound-deficient mice were found to be decreased compared with those of WT. Regarding the parameters of bone formation, the mineral apposition rate and bone

FIGURE 2. **Radiological analysis of adult**
Bmp2+/−;Bmp6−/− mice. A, plain radiographs
of the femurs (*upper panels*) and tibias (*lower panels*) from WT, Bmp2+/−, Bmp6−/−, and Bmp2+/
−;Bmp6−/− mice at 9 weeks of age. B, BMD of the
whole femurs from WT, Bmp2+/−, Bmp6+/−,
Bmp6−/−, Bmp2+/−;Bmp6+/−, and Bmp2+/−;
Bmp6−/− mice at 9 weeks of age. Data are
expressed as mean ± S.E. for 12 bones/group. *,
$p < 0.01$ *versus* the rest. C, three-dimensional CT
analysis of the distal epiphysis of the femurs from
WT (*upper panels*) and Bmp2+/−;Bmp6−/− mice
(*lower panels*) at 9 weeks of age. D, plain radiographs of the calvarias from WT, Bmp2+/−,
Bmp6−/−, and Bmp2+/−;Bmp6−/− mice at 9
weeks of age. E, BMD of the calvarias from WT,
Bmp2+/−, Bmp6+/−, Bmp6−/−, Bmp2+/−;
Bmp6+/−, and Bmp2+/−;Bmp6−/− mice at 9
weeks of age.

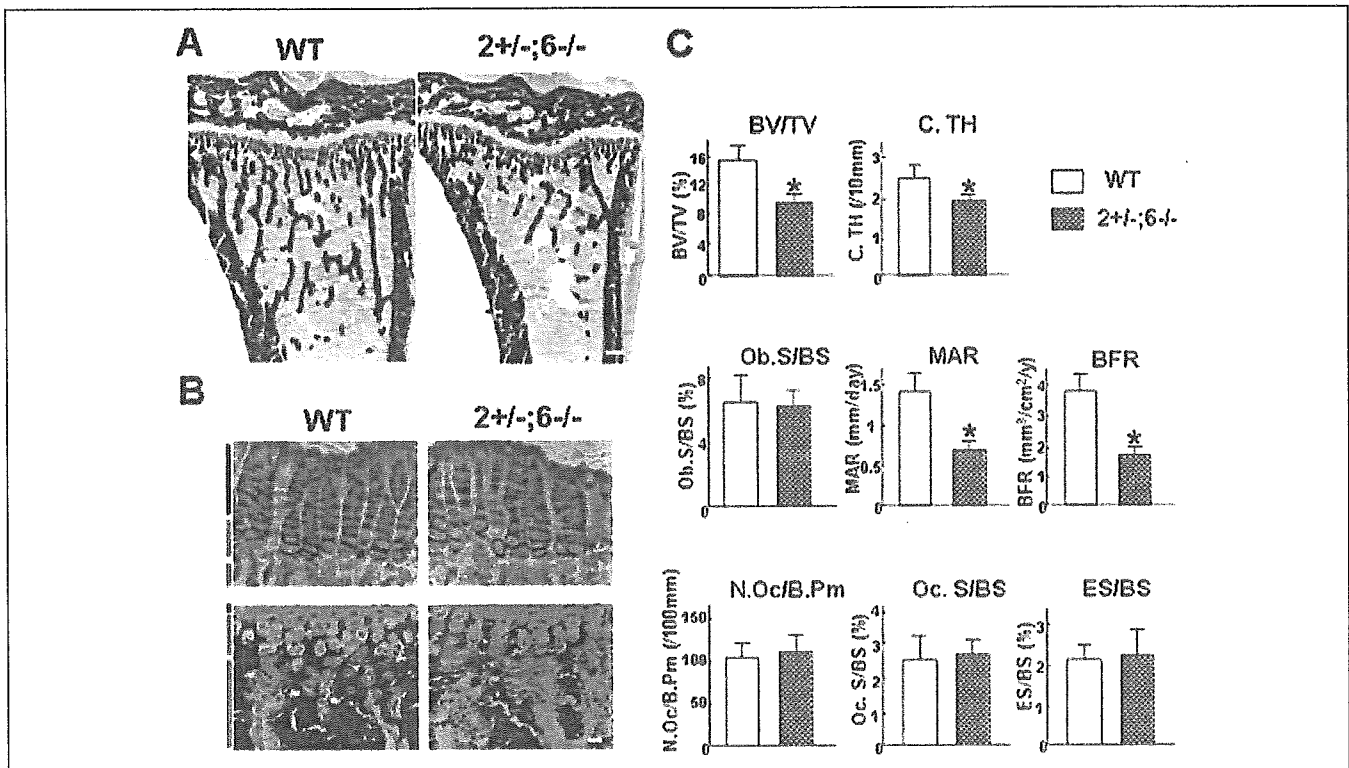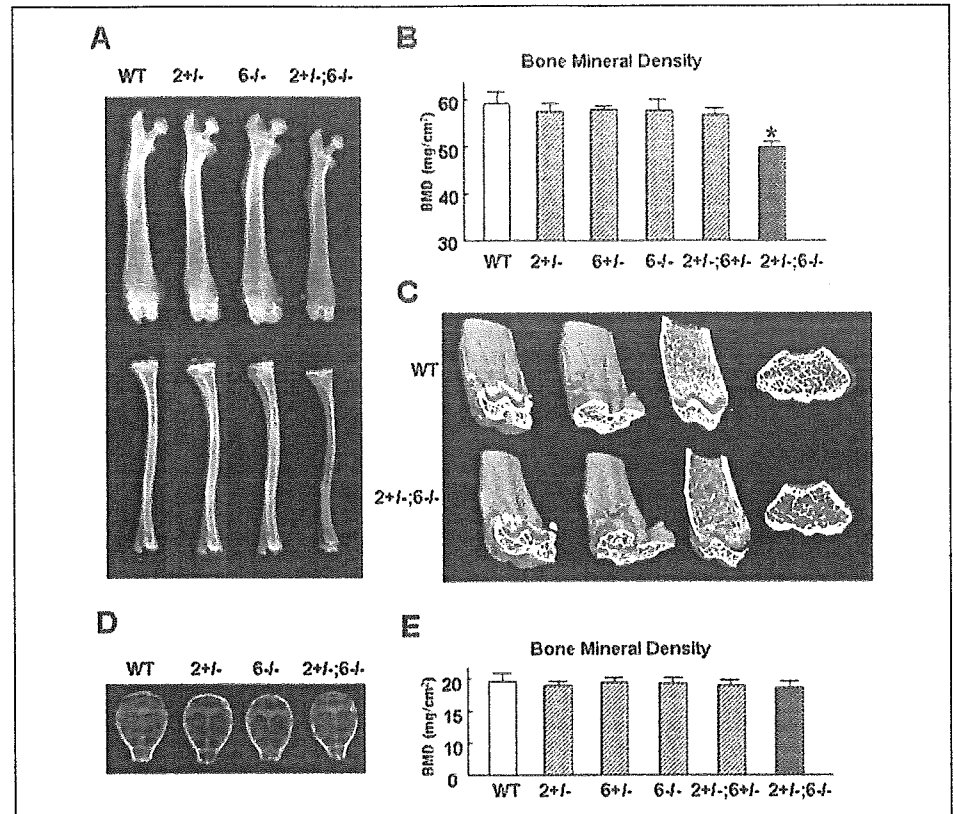FIGURE 3. **Histological analysis of adult** *Bmp2+/−;Bmp6−/−* **mice.** A, von Kossa staining of the tibia sections from WT and Bmp2/−;Bmp6−/− mice at 9 weeks of age. *Scale bar,*
300 μm. B, toluidine blue staining (upper panels) and von Kossa staining (*lower panels*) of the tibia growth plate sections from WT and Bmp2+/−;Bmp6−/− mice at 9 weeks of age.
Blue, green, and *red bars* indicate the layer of proliferating chondrocytes, the layer of hypertrophic chondrocytes, and the primary spongiosa, respectively. *Scale bar,* 20 μm. C, bone
histomorphometric analysis of the tibias from WT and Bmp2+/−;Bmp6−/− mice at 9 weeks of age. *BV/TV,* bone volume per tissue volume; *C.Th,* cortical bone thickness; *Ob.S/BS,*
osteoblast surface per bone surface; *MAR,* mineral apposition rate; *BFR/BS,* bone formation rate per bone surface; *N.Oc/B.Pm,* number of osteoclasts per 100 mm of bone perimeter;
Oc.S/BS, osteoclast surface per bone surface; *ES/BS,* erosive surface per bone surface. Data are expressed as the mean ± S.E. of 8 mice per genotype. *, $p < 0.05$ *versus* WT.

FIGURE 4. **Radiological and histological analyses of the fracture callus.** *A,* plain radiographs of the fractured femurs at 18 days after the surgery from WT, *Bmp2+/−, Bmp6−/−,* and *Bmp2+/−; Bmp6−/−* mice at 9 weeks of age. *B,* measurement of the calcified area and the bone mineral content of the callus at the fracture site measured by single energy x-ray absorptiometry. Data are expressed as the mean ± S.E. of 8 mice per genotype. *, $p <$ 0.01 *versus* WT. *C,* H&E staining (*upper panels*) and toluidine blue staining (*lower panels*) of the fractured femur sections from WT, *Bmp2+/−, Bmp6−/−,* and *Bmp2+/−;Bmp6−/−* mice. *Red* and *blue bars* indicate the peripheral part and the central part of the fracture site, respectively. *Scale bar,* 300 μm. *D,* the ratio of the calcified area to the total area (*CA/TA*) in the peripheral part (*left panel*) and central part (*right panel*) of the fracture site histologically measured by NIH Image. Data are expressed as the mean ± S.E. of 8 mice per genotype. *, $p <$ 0.01 *versus* WT. *E,* H&E staining and immunohistochemical analysis with anti-type X collagen and MMP-13 antibodies of the sections of the fractured femurs at 5 and 7 days after the surgery from WT and *Bmp2+/−;Bmp6−/−* mice. The *boxed areas* in the *left panels* showing MMP-13 expression are magnified in the *right panels. Arrowheads* indicate MMP-13 expression, which is stained *brown. Scale bar,* 300 μm.
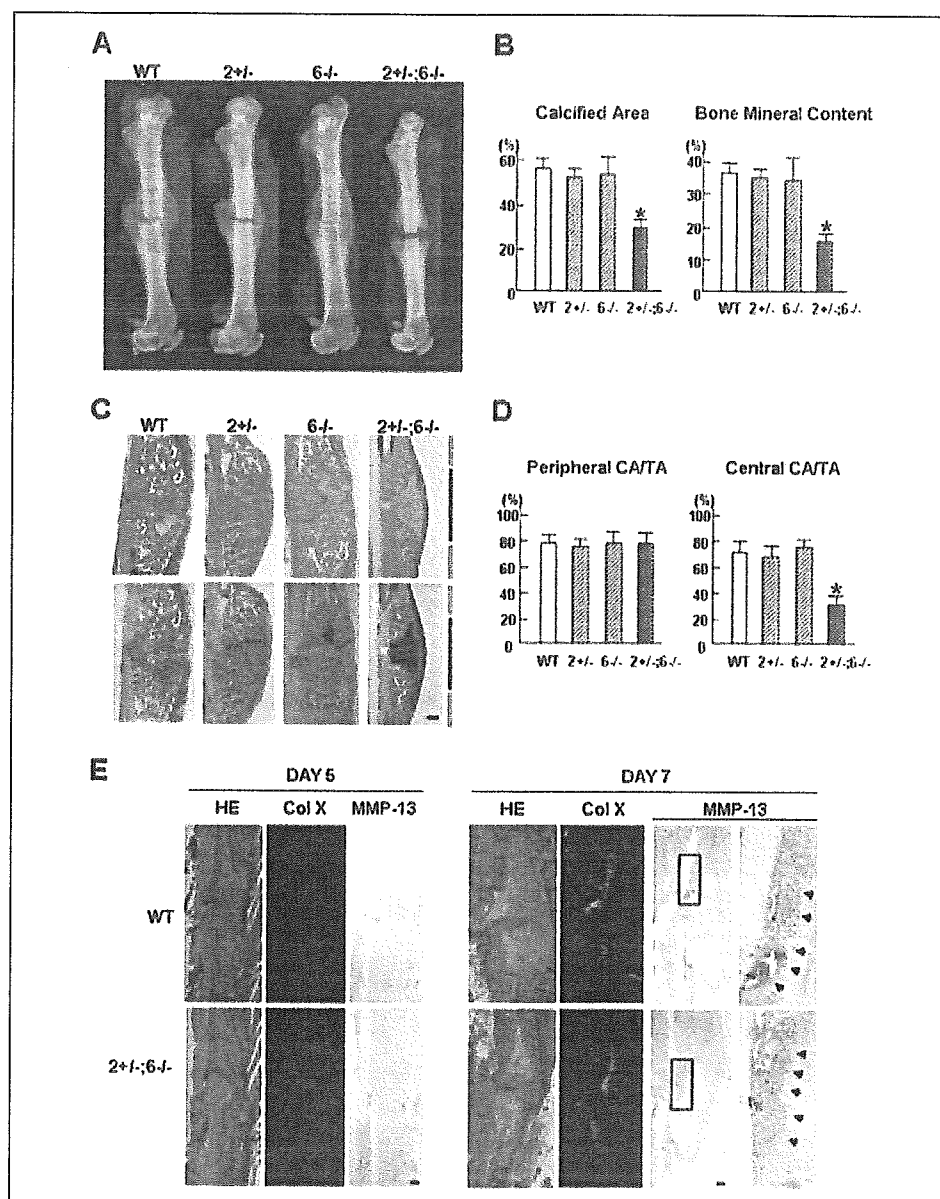
formation rate per bone surface were markedly decreased with no remarkable difference in the osteoblast number expressed by Ob.S/BS. On the other hand, the parameters of bone resorption were normal. These data suggest that the bone loss in the compound-deficient mice is caused by the inhibition of the bone formation because of the impaired osteoblast function.

To rule out the possibility that the bone loss of these mice was caused by general conditions, such as renal failure or abnormal calcium homeostasis, the serum biochemical data were analyzed. There was no remarkable difference in the serum creatinine, calcium, or inorganic phosphorus between WT and compound-deficient mice (data not shown). Urinary deoxypyridinoline, a marker for bone resorption, showed no remarkable difference between the two groups, confirming the bone histomorphometric data (data not shown).

Bone Fracture Healing in Bmp2+/−;Bmp6−/− Mice—The data so far suggest that the combination of the endogenous BMP2 and BMP6 plays an important role in bone formation under physiological conditions. To further investigate the effects of the compound loss of *Bmp2*

and *Bmp6* on bone formation under pathological conditions, we generated fractures at the midshaft of the femurs and compared the healing process among WT, *Bmp2+/−, Bmp6−/−,* and *Bmp2+/−;Bmp6−/−* mice. Radiological analysis at 18 days after the fracture showed substantial calcified callus formation in WT, *Bmp2+/−,* and *Bmp6−/−* mice (Fig. 4A). On the other hand, in the compound-deficient mice, fracture healing was delayed, and the size of the calcified callus was reduced. To quantify the extent of the callus formation, the % gain of the calcified area and the % gain of bone mineral content in the fractured and control femurs were measured using a bone densitometer (Fig. 4B). Although no significant difference was observed among WT, *Bmp2+/−,* and *Bmp6−/−* mice at 18 days after the fracture, both parameters were markedly reduced in the compound-deficient mice. When histological sections were stained with H&E and toluidine blue to distinguish between the bone and cartilage tissues, the total callus size was reduced, and a massive cartilaginous callus containing hypertrophic chondrocytes persisted in the compound-deficient mice. During fracture healing, new bone is known to be formed through two pathways: the endo-

FIGURE 5. **Osteogenic differentiation in the cultures of** *Bmp2+/−;Bmp6−/−* **bone marrow cells.** *A,* *in situ* hybridization of the tibia sections from WT mouse with mouse BMP2, BMP6, and type I collagen antisense probes. *Left panels,* bright field views; *right panels,* dark field views. *Blue, green,* and *red bars* indicate the layer of proliferating chondrocytes, the layer of hypertrophic chondrocytes, and the primary and secondary spongiosas, respectively. *Lower panels* are the magnified views of the *boxed areas* in the *upper panels. Scale bar,* 100 μm in the *upper panels* and 20 μm in the *lower panels. B,* bone marrow cells were isolated from 3-week-old WT and *Bmp2+/−; Bmp6−/−* mice and cultured in serum-free osteogenic medium in the presence or absence of exogenous rhBMP2 (200 ng/ml). Two weeks after confluence, ALP, Alizarin red S, and von Kossa stainings were performed. *C,* expression of osteopontin and osteocalcin mRNAs was determined by real-time RT-PCR on the above mentioned marrow cells. Data are expressed as the mean ± S.E. of 6 wells per group. *, $p < 0.01$, significant stimulation by rhBMP2. *D,* temporal profiles of the numbers of CFU-F, CFU-ALP, and bone nodules using WT and *Bmp2+/−;Bmp6−/−* bone marrow cells. Bone marrow cells were isolated from 3-week-old mice, then cultured in serum-free osteogenic medium in the presence or absence of exogenous rhBMP2 (200 ng/ml). After 5, 10, and 15 days, ALP and von Kossa stainings were performed. Data are expressed as mean ± S.E. for 6 wells per group. *, $p < 0.01$, significant stimulation by rhBMP2.
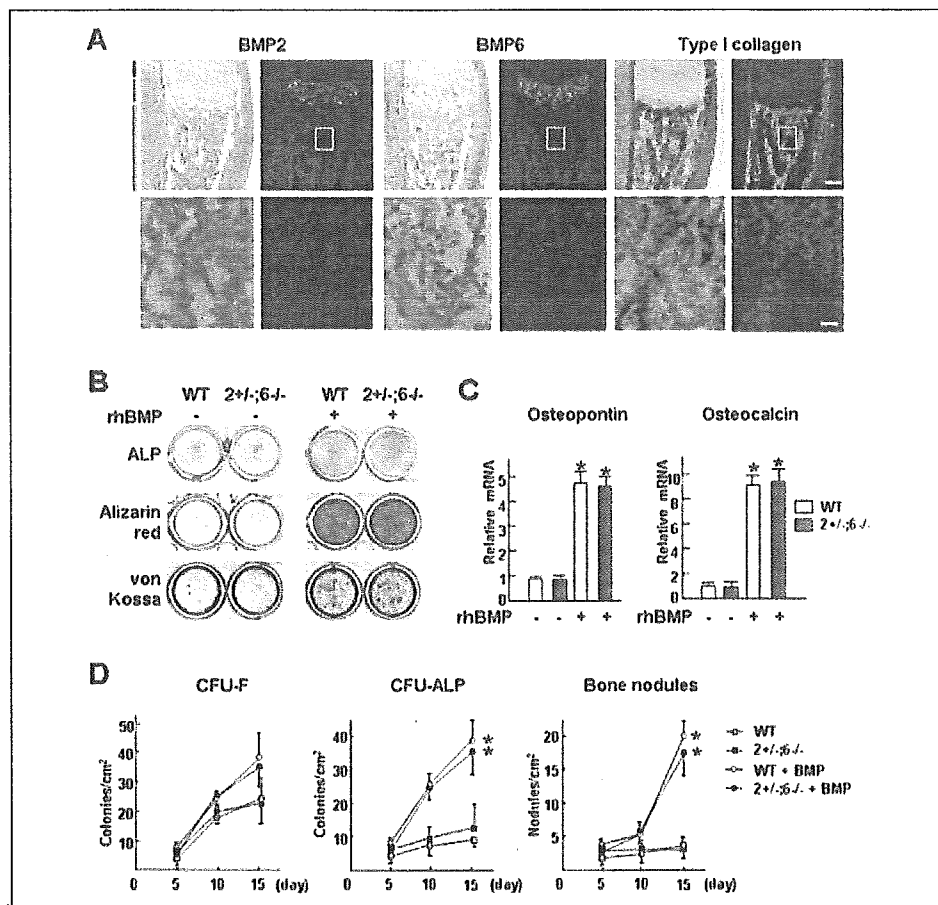
chondral bone formations in the center and the intramembranous bone formation in the periphery of the callus (17). To distinguish these two pathways, we divided the callus into three equal portions along the axis of the bone, and designated the distal and proximal ⅓ portions as the peripheral part, and the middle ⅓ portion as the central part. The measurement of the ratio of the calcified area to the total area (CA/TA) of the histological sections using NIH Image revealed that calcification in the central part, but not in the peripheral part, was significantly reduced in the compound-deficient mice compared with that in WT (Fig. 4D), indicating that the endochondral, not intramembranous, bone formation, was defective in the compound-deficient mice. To investigate whether the delayed fracture healing in *Bmp2+/−;Bmp6−/−* mice was caused by a delay in terminal differentiation of chondrocytes, we examined the earlier stages of fracture healing in WT and compound-deficient mice. H&E staining and immunohistochemical analysis with anti-type X collagen and MMP-13 antibodies showed that no hypertrophic differentiation occurred in either group at 5 days after the fracture (Fig. 4E). At 7 days after the fracture, terminal hypertrophic differentiation of chondrocytes determined by expression of MMP-13 and intramembranous bone formation occurred in both groups.

In Vitro Bone Marrow Differentiation Assay—The current results support the view that the endogenous BMP2 and BMP6 play vital roles in bone formation under physiological and pathological conditions. *In situ* hybridization analysis indicated that, in comparison with the expression in hypertrophic chondrocytes, there was little, if any, expression of BMP2 and BMP6 in bone and bone marrow cells including osteoblasts that were marked by the strong expression of the type I collagen (Fig. 5A). However, we still could not rule out the possibility

that a small amount of BMP2 and BMP6 secreted from bone and bone marrow cells might act in an autocrine or paracrine fashion to modulate the osteoblast function. To test this possibility, we isolated bone marrow cells including osteoblasts from 3-week-old mice, cultured them in serum-free osteogenic medium, and assessed their osteogenic ability. ALP, Alizarin red S, and von Kossa stainings revealed no difference in the basal osteogenic ability between WT and *Bmp2+/−;Bmp6−/−* cells (Fig. 5B). Upon treatment with rhBMP2 (200 ng/ml), both WT and the compound-deficient cells responded well to the same extent (Fig. 5B). The real-time RT-PCR analysis of osteopontin and osteocalcin, markers for osteoblasts, revealed no difference between the two genotypes (Fig. 5C). The quantitative analysis of the numbers of CFU-F, CFU-ALP, and bone nodules using bone marrow cells isolated from 3-week-old WT and compound-deficient mice revealed no difference in the basal osteogenic ability (Fig. 5D). Upon treatment with rhBMP2 (200 ng/ml), both WT and the compound-deficient cells responded well to the same extent in terms of the numbers of CFU-ALP and bone nodules (Fig. 5D). These data suggest that the endogenous BMP2 and BMP6 secreted from bone marrow cells do not contribute to the regulation of bone formation.

DISCUSSION

Because hypertrophic chondrocytes induce bone formation in the primary spongiosa and the perichondrium during endochondral bone formation, the present study hypothesized that endogenous BMPs secreted from these chondrocytes might be involved in bone formation. Although there have been a number of reports describing the expression patterns of BMPs in the growth plate (13), they do not particularly

focus on these chondrocytes. To obtain physiologically relevant data on the role of the endogenous BMPs during bone formation, we screened for BMPs expressed by these chondrocytes to find that BMP2 and BMP6 were the main subtypes and analyzed the effects of their loss on bone formation.

Fetal *Bmp2+/−;Bmp6−/−* mice exhibited a reduced bone formation in the primary spongiosa, probably because of reduced bone formation and/or stimulation of bone resorption. We think the latter possibility rather unlikely, because the number of osteoclasts was not increased in the compound-deficient mice. The expression of the type I collagen, a marker for both early and late osteoblasts, showed no reduction, suggesting that the differentiation of osteoblasts from the precursor cells was not affected. The growth plates of these mice were smaller, but the proportions of distinct layers were maintained; in addition, the expressions of type II and X collagens were not changed, and hypertrophic chondrocytes mineralized the surrounding cartilaginous matrix to the same extent as WT. There was no difference in the onset of terminal differentiation. These data suggest that there is little, if any, abnormality in the chondrocyte differentiation. The data for adult mice concur with those of fetal mice; bone formation was reduced because of the impaired function of the osteoblasts with no change in their number, whereas the bone resorption markers were all normal. Taken together, these findings provide evidence that the combination of the endogenous BMP2 and BMP6 is vital for bone formation in both the fetal and adult life stages.

In line with our results are those of transgenic mice expressing a dominant-negative form of the *BMP receptor 1B* (*BMPR-1B*) under the control of the type I collagen promoter (24). They were smaller than WT and showed impairment of postnatal bone formation with the number of osteoblasts and the parameters of bone resorption unchanged, suggesting that the osteoblast function was impaired. In addition, transgenic mice lacking the *BMP receptor 1A* (*BMPR-1A*) specifically in osteoblasts using the Cre/loxP system under the control of the Og2 promoter also exhibited a low bone mass because of the impaired osteoblast function (25). The bone phenotypes of these genetically manipulated mice, of which the osteoblast could not transduce normal BMP signaling, are similar to those of *Bmp2+/−;Bmp6−/−* mice. These data suggest that osteoblasts require endogenous BMPs to provide their full function *in vivo*, but are not informative on the subtype and the origin of such BMPs. Our data suggest that BMP2 and BMP6 are two of them.

One question, however, still remained as to where BMP2 and BMP6 came from to act on the osteoblasts. There were three possibilities. First, they came from hypertrophic chondrocytes. Second, they came from bone and bone marrow cells in an autocrine or paracrine fashion. Third, they came from other cell sources at a distance in an endocrine fashion. *In situ* hybridization analysis of the developing bone showed that BMP6 was exclusively expressed in hypertrophic chondrocytes and that BMP2 was strongly expressed in hypertrophic chondrocytes and marginally in the osteoblasts. Bone marrow cells obtained from *Bmp2+/−; Bmp6−/−* mice showed the same osteogenic ability as WT both at the basal status and in response to the exogenous BMP2. Furthermore, intramembranous bone formation in the calvaria was not affected in *Bmp2+/−;Bmp6−/−* mice. These data favor the first possibility. To strictly prove this, however, a further study using the tissue-specific ablation of the *Bmp2* and *Bmp6* genes in hypertrophic chondrocytes is needed. In addition, we should be careful in extrapolating the results of murine experiments to humans, because the growth plate, the source of hypertrophic chondrocytes, in humans disappears at puberty, whereas that of mice persists throughout life.

As for the small size of the growth plate, it may be related to the decreased axial growth of the mutant mice. It may be that the loss of BMP2 and BMP6 affects the size of the mesenchymal condensations and/or the proliferation rate of the chondrocytes. Alternatively, the osteoblast dysfunction caused by the compound loss of these BMPs may elicit a decrease in the axial bone growth, because there is a report that the ablation of the osteoblasts led to skeletal growth arrest (26). A further study is needed to clarify these issues.

In the fracture model, the cartilaginous callus was almost completely replaced by newly formed bone tissue in WT mice, whereas a massive cartilaginous callus persisted in *Bmp2+/−;Bmp6−/−* mice. When the callus was divided into the central and peripheral part, mineralization of the central part, where the endochondral bone formation prevailed, was reduced. These data suggest that the replacement of cartilaginous callus by bone is affected in the compound-deficient mice, which is in line with the data for physiological bone formation. It is noteworthy that the total callus size of the compound-deficient mice was smaller than that of WT. This may be because of the same cause of the smaller size of the growth plate.

A previous study of chimeric mice containing both WT and *Ihh−/−*; parathyroid hormone/parathyroid hormone-related peptide receptor−/− cells revealed that Ihh synthesized by the prehypertrophic and hypertrophic chondrocytes was locally required for the induction of bone formation in the adjacent perichondrium (8). In these chimeric mice, although both BMP2 and BMP6 were strongly expressed by the ectopic *Ihh−/−*;parathyroid hormone/parathyroid hormone-related peptide receptor−/− hypertrophic chondrocytes, the ectopic bone formation did not occur, suggesting that BMPs alone were not sufficient to induce physiological bone formation. In addition, blocking of Hh signaling inhibited the BMP2-induced osteogenic differentiation in mouse limb bud cell line MLB13MYC clone 17 (10), suggesting the presence of synergistic interactions between Ihh and BMPs. In the present study, the lack of one allele of the *Bmp2* gene and both alleles of the *Bmp6* gene caused a reduction in bone formation because of the osteoblast dysfunction. Taken together, we think it likely that BMP2 and BMP6 expressed by hypertrophic chondrocytes act in synergy with Ihh for physiological bone formation.

BMP2 and BMP6 have been reported to form a heterodimer, which was more potent for induction of osteogenic differentiation than the BMP2 homodimer or BMP6 homodimer (27). To assess the role of the BMP2/BMP6 heterodimer *in vivo*, we analyzed the bone formation of *Bmp6−/−* mice. The BMD of *Bmp6−/−* mice, which were thought to have no BMP2/BMP6 heterodimer, was similar to that of WT. In addition, the fracture model did not reveal any difference between WT and *Bmp6−/−* mice. These data suggest that, although the BMP2/BMP6 heterodimer is more potent than the BMP2 or BMP6 homodimers in *in vitro* or implant experiments, the BMP2/BMP6 heterodimer may not have a physiologically relevant role in the bone formation.

In conclusion, the combination of BMP2 and BMP6 plays pivotal roles in bone formation under both physiological and pathological conditions. To the best of our knowledge, this is the first report to show that endogenous BMPs are important for *in vivo* bone formation.

REFERENCES

1. Wozney, J. M., Rosen, V., Celeste, A. J., Mitsock, L. M., Whitters, M. J., Kriz, R. W., Hewick, R. M., and Wang, E. A. (1988) *Science* 242, 1528–1534
2. Urist, M. R. (1965) *Science* 150, 893–899
3. Kawabata, M., and Miyazono, K. (2000) in *Skeletal Growth Factors* (Ernesto Canalis, M. D., ed) pp. 269–290, Lippincott Williams & Wilkins, Philadelphia
4. Zhao, G. Q. (2003) *Genesis* 35, 43–56
5. Karsenty, G. (2000) in *Skeletal Growth Factors* (Ernesto Canalis, M. D., ed) pp. 291–310, Lippincott Williams & Wilkins, Philadelphia
6. Kronenberg, H. M. (2003) *Nature* 423, 332–336
7. Chung, U. I. (2004) *Endocr. J.* 51, 19–24

8. Chung, U. I., Schipani, E., McMahon, A. P., and Kronenberg, H. M. (2001) *J. Clin. Investig.* **107,** 295–304
9. Takeda, S., Bonnamy, J. P., Owen, M. J., Ducy, P., and Karsenty, G. (2001) *Genes Dev.* **15,** 467–481
10. Long, F., Chung, U. I., Ohba, S., McMahon, J., Kronenberg, H. M., and McMahon, A. P. (2004) *Development* **131,** 1309–1318
11. Long, F., Zhang, X. M., Karp, S., Yang, Y., and McMahon, A. P. (2001) *Development* **128,** 5099–5108
12. Zhang, H., and Bradley, A. (1996) *Development* **122,** 2977–2986
13. Solloway, M. J., Dudley, A. T., Bikoff, E. K., Lyons, K. M., Hogan, B. L., and Robertson, E. J. (1998) *Dev. Genet.* **22,** 321–339
14. Komori, T., Yagi, H., Nomura, S., Yamaguchi, A., Sasaki, K., Deguchi, K., Shimizu, Y., Bronson, R. T., Gao, Y. H., Inada, M., Sato, M., Okamoto, R., Kitamura, Y., Yoshiki, S., and Kishimoto, T. (1997) *Cell* **89,** 755–764
15. Lee, K., Deeds, J. D., and Segre, G. V. (1995) *Endocrinology* **136,** 453–463
16. Shimoaka, T., Kamekura, S., Chikuda, H., Hoshi, K., Chung, U. I., Akune, T., Maruyama, Z., Komori, T., Matsumoto, M., Ogawa, W., Terauchi, Y., Kadowaki, T., Nakamura, K., and Kawaguchi, H. (2004) *J. Biol. Chem.* **279,** 15314–15322
17. Kawaguchi, H., Kurokawa, T., Hanada, K., Hiyama, Y., Tamura, M., Ogata, E., and Matsumoto, T. (1994) *Endocrinology* **135,** 774–781
18. Aubin, J. E. (1998) *J. Cell. Biochem.* **30–31,** (suppl.) 73–82
19. Malaval, L., and Aubin, J. E. (2001) *J. Cell. Biochem.* **81,** 63–70
20. Nishida, S., Tsurukami, H., Sakai, A., Sakata, T., Ikeda, S., Tanaka, M., Ito, M., and Nakamura, T. (2002) *Bone* **30,** 872–879
21. D'Angelo, M., Yan, Z., Nooreyazdan, M., Pacifici, M., Sarment, D. S., Billings, P. C., and Leboy, P. S. (2000) *J. Cell. Biochem.* **77,** 678–693
22. Jimenez, M. J., Balbin, M., Alvarez, J., Komori, T., Bianco, P., Holmbeck, K., Birkedal-Hansen, H., Lopez, J. M., and Lopez-Otin, C. (2001) *J. Cell Biol.* **155,** 1333–1344
23. Kamekura, S., Hoshi, K., Shimoaka, T., Chung, U., Chikuda, H., Yamada, T., Uchida, M., Ogata, N., Seichi, A., Nakamura, K., and Kawaguchi, H. (2005) *Osteoarthritis Cartilage* **13,** 632–641
24. Zhao, M., Harris, S. E., Horn, D., Geng, Z., Nishimura, R., Mundy, G. R., and Chen, D. (2002) *J. Cell Biol.* **157,** 1049–1060
25. Mishina, Y., Starbuck, M. W., Gentile, M. A., Fukuda, T., Kasparcova, V., Seedor, J. G., Hanks, M. C., Amling, M., Pinero, G. J., Harada, S., and Behringer, R. R. (2004) *J. Biol. Chem.* **279,** 27560–27566
26. Corral, D. A., Amling, M., Priemel, M., Loyer, E., Fuchs, S., Ducy, P., Baron, R., and Karsenty, G. (1998) *Proc. Natl. Acad. Sci. U. S. A.* **95,** 13835–13840
27. Israel, D. I., Nove, J., Kerns, K. M., Kaufman, R. J., Rosen, V., Cox, K. A., and Wozney, J. M. (1996) *Growth Factors* **13,** 291–300

Insulin Receptor Substrate-1 Is Required for Bone Anabolic Function of Parathyroid Hormone in Mice

Masayuki Yamaguchi,* Naoshi Ogata, Yusuke Shinoda, Toru Akune, Satoru Kamekura, Yasuo Terauchi, Takashi Kadowaki, Kazuto Hoshi, Ung-Il Chung, Kozo Nakamura, and Hiroshi Kawaguchi

Departments of Sensory and Motor System Medicine (M.Y., N.O., Y.S., T.A., S.K., K.H., U.-I.C., K.N., H.K.) and Metabolic Diseases (Y.T., T.K.), Faculty of Medicine, University of Tokyo, Tokyo 113-8655, Japan

Bone anabolic action of PTH has been suggested to be mediated by induction of IGF-I in osteoblasts; however, little is known about the molecular mechanism by which IGF-I leads to bone formation under the PTH stimulation. This study initially confirmed in mouse osteoblast cultures that PTH treatment increased IGF-I mRNA and protein levels and alkaline phosphatase activity, which were accompanied by phosphorylations of IGF-I receptor, insulin receptor substrate (IRS)-1 and IRS-2, essential adaptor molecules for the IGF-I signaling. To learn the involvement of IRS-1 and IRS-2 in the bone anabolic action of PTH *in vivo*, *IRS-1−/−* and *IRS-2−/−* mice and their respective wild-type littermates were given daily injections of PTH (80 μg/kg) or vehicle for 4 wk. In the wild-type mice, the PTH injection increased bone mineral densities of the femur, tibia, and vertebrae by 10–20% without altering the serum IGF-I level. These stimulations were similarly seen in *IRS-2−/−* mice; however, they were markedly suppressed in *IRS-1−/−* mice. Although the PTH anabolic effects were stronger on trabecular bones than on cortical bones, the stimulations on both bones were blocked in *IRS-1−/−* mice but not in *IRS-2−/−* mice. Histomorphometric and biochemical analyses showed an increased bone turnover by PTH, which was also blunted by the IRS-1 deficiency, though not by the IRS-2 deficiency. These results indicate that the PTH bone anabolic action is mediated by the activation of IRS-1, but not IRS-2, as a downstream signaling of IGF-I that acts locally as an autocrine/paracrine factor. (*Endocrinology* 146: 2620–2628, 2005)

A NABOLIC EFFECTS of PTH on bone have attracted considerable clinical attention and led to the approval of PTH for osteoporosis treatment (1–3). Although it has been well established that intermittent administration of PTH exerts potent anabolic effects on bone in animals and humans (4), the underlying mechanism is still controversial and unclear. PTH is reported to increase production of osteoprogenitors and differentiation of osteoblasts from an existing pool of osteoprogenitors and to decrease apoptosis of pre-existing osteoblasts (5–7). Accumulated evidence has shown that IGF-I is an attractive candidate as a mediator for some or all of the anabolic actions of PTH on bone, in that PTH stimulates IGF-I production by osteoblastic cells (8, 9) and IGF-1 can reproduce the effects of PTH on osteoblast proliferation, differentiation, and survival (10). From *in vitro* studies, IGF-I-blocking antibodies inhibited collagen synthesis and alkaline phosphatase (ALP) activity, as well as the expression of osteocalcin mRNA induced by PTH stimulation on osteoblasts (11, 12). Furthermore, PTH anabolic actions were suppressed when administered to IGF-I-deficient

mice (13, 14), suggesting the importance of the IGF-I signaling *in vivo*.

IGF-I initiates cellular responses by binding to its cell-surface receptor tyrosine kinase IGF-I receptor, which then activates essential adaptor molecule insulin receptor substrates (IRS's) followed by downstream signaling pathways like phosphatidylinositol-3 kinase (PI3K)/Akt and MAPKs (15). The mammalian IRS family contains at least four members: ubiquitous IRS-1 and IRS-2, adipose tissue-predominant IRS-3, and IRS-4 which is expressed in the thymus, brain, and kidney. We previously reported that IRS-1 and IRS-2 are expressed in bone (16, 17). Our further studies on mice lacking the IRS-1 gene (*IRS-1−/−* mice) or the IRS-2 gene (*IRS-2−/−* mice) revealed that these knockout mice exhibited severe osteopenia with distinct mechanisms: *IRS-1−/−* mice showed a low bone turnover in which both bone formation and resorption were decreased (16), whereas *IRS-2−/−* mice showed an uncoupling status with decreased bone formation and increased bone resorption (17). It therefore seems that under physiological conditions, IRS-1 is important for maintaining bone turnover, whereas IRS-2 is important for retaining the predominance of anabolic function over catabolic function of osteoblasts.

To learn the molecular mechanism by which IGF-I leads to bone formation under the PTH stimulation, the present study investigated the role of IRS-1 and IRS-2 in mediating the anabolic effects of recombinant human PTH(1–34) on bone. We first studied the effects of PTH on the IGF-I related molecules in cultured mouse osteoblasts and examined skeletal responses to PTH in *IRS-1−/−* and *IRS-2−/−* mice.

2620

Materials and Methods

Animals

Mice with the original C57BL6/CBA hybrid background were generated and maintained as reported previously (16, 17). In each experiment, homozygous wild-type (WT) and *IRS-1−/−* male mice, as well as homozygous WT and *IRS-2−/−* male mice, that were littermates generated from the intercross between heterozygous mice were compared. All mice were kept in plastic cages under standard laboratory conditions with a 12-h dark, 12-h light cycle, a constant temperature of 23 C, and humidity of 48%. The mice were fed a standard rodent diet (CE-2; CLEA Japan, Inc., Tokyo, Japan) containing 25.2% protein, 4.6% fat, 4.4% fiber, 6.5% ash, 3.44 kcal/g, 2.5 IU vitamin D_3/g, 1.09% calcium, and 0.93% phosphorus with water *ad libitum*. All animal experiments were reviewed and approved by the University of Tokyo, Faculty of Medical Animal Care and Use Committee, before the study.

Osteoblast cultures

Osteoblasts were isolated from calvariae of neonatal WT, *IRS-1−/−*, and *IRS-2−/−* littermates. Calvariae were digested for 10 min, 5 times, at 37 C in an enzyme solution containing 0.1% collagenase and 0.2% dispase. Cells isolated by the last four digestions were combined as an osteoblast population and cultured in αMEM (Invitrogen, Carlsbad, CA) containing 10% FBS (HyClone Laboratories, Inc., Logan, UT) and 50 μg/ml ascorbic acid (Sigma-Aldrich Corp., St. Louis, MO).

For real-time quantitative RT-PCR analysis, primary osteoblasts were inoculated at a density of 1×10^4 cells/well in a 24-multiwell plate, and cultured in the medium above, with or without 100 nM recombinant human PTH(1–34) (Sigma-Aldrich Corp.) for 14 d. Total RNA was extracted with an ISOGEN kit (Wako Pure Chemical Industries Ltd., Osaka, Japan), according to the manufacturer's instructions. One microgram of RNA was reverse-transcribed using a Takara RNA PCR Kit, version 2.1 (Takara Shuzo Co., Shiga, Japan), to make single-stranded cDNA. The ABI Prism Sequence Detection System 7000 and Primer Express Software (Applied Biosystems, Foster City, CA) were used for PCR amplification and quantitative analysis, respectively. For the IGF-I gene, a set of primers was designed using sequences obtained from the GenBank as follows: 5'GACAGATACARRCTGTGCTCA-3' and 5'-CT-GAAGCTTGCTAACATCGC-3'. The PCR consisted of QuantiTect SYBR Green Master Mix (QIAGEN, Tokyo, Japan), 0.3 μM specific primers, and 20 ng cDNA.

For the IGF-I protein level measurement, primary osteoblasts were cultured, as described above, for 14 d, and the free IGF-I concentration in the culture media was measured with a Non-Extraction IGF-I ELISA kit (Diagnostic Systems Laboratories, Inc., Sparks, MD).

For ALP activity measurement, primary osteoblasts were cultured in the medium above with or without 10 ng/ml recombinant mouse IGF-I (Sigma-Aldrich Corp.) and 5 nM antimouse IGF-I antibody (Sigma-Aldrich Corp.). At 14 d of culture, cells were sonicated in 10 mM Tris-HCl buffer (pH 8.0) containing 1 mM $MgCl_2$ and 0.5% Triton X-100, and ALP activity in the lysate was measured using an ALP assay kit (Wako Pure Chemical Industries Ltd.). The protein content was determined using BCA protein assay reagent (Pierce Chemical Co., Rockford, IL).

Immunoprecipitation and immunoblotting

After stimulation by 100 nM PTH for the indicated time, cultured osteoblasts were lysed with TNE buffer (10 mM Tris-HCl, 150 mM NaCl, 1% NP-40, 1 mM EDTA, 10 mM NaF, 2 mM Na_3VO_4, 1 mM aminoethyl-benzenesulfonyl fluoride, and 10 μg/ml aprotinin). A part of the cell lysates (100 μg) was immunoprecipitated with an antiphosphotyrosine antibody, an antimouse IGF-I receptor antibody, an antimouse insulin receptor antibody, an antimouse IRS-1 antibody, or an antimouse IRS-2 antibody (all from Upstate Biotechnology, Inc., Waltham, MA) conjugated to protein G-Sepharose (Invitrogen) for 4 h at 4 C. The cell lysates with or without the immunoprecipitation that contained an equivalent amount of protein (20 μg) were electrophoresed by 8% SDS-PAGE and transferred to nitrocellulose membrane. After blocking with 5% BSA solution, they were incubated with the antibodies above, and the immunoreactive bands were stained using the ECL chemiluminescence reaction (Amersham, Arlington Heights, IL). The intensity of each band was measured by densitometry (Bio-Rad Laboratories, Inc., Richmond,

CA) and was expressed as the mean value of five independent experiments.

PTH treatment on mice

IRS-1−/− mice and their littermates and *IRS-2−/−* mice and their littermates (males, all n = 10) received either PTH (80 μg/kg body weight) or vehicle (PBS) by sc injection every day for 4 wk beginning at 10 wk of age. Blood samples were collected by heart puncture under nembutal (Dainippon Pharmaceutical Co., Ltd., Osaka, Japan) anesthesia before being killed. For radiological and histological analyses, animals were killed after 4 wk of PTH treatment by diethylether. The right femurs and tibiae were obtained for bone densitometry, and the left femurs and tibiae for peripheral quantitative computerized tomography (pQCT) and histological analyses, respectively. Lumbar vertebral bodies from L2–L5 were also obtained for bone densitometry.

Bone densitometry and pQCT

Bone mineral density (BMD; milligrams per square centimeter) of the right femur, tibiae, and L2–L5 vertebral bodies was determined using dual-energy x-ray absorptiometry (PIXImus Mouse Densitometer; Lunar Corp., Madison, WI) according to the manufacturer's instructions. Computerized tomography was performed with a pQCT analyzer (XCT Research SA+; Stratec Medizintechnik GmbH, Pforzheim, Germany) operating at a resolution of 80 μm. Metaphyseal pQCT scans of the left femurs were performed to measure the trabecular volumetric BMD. The scan was positioned in the metaphysis at 1.2 mm proximal from the distal growth plate. Because this area contains trabecular and cortical bones, the trabecular bone region was defined by setting the threshold to 395 mg/cm³. Middiaphyseal pQCT scans of the left femurs were performed to determine the cortical thickness. The middiaphyseal region of femurs in mice contains mostly cortical bone. The cortical bone region was defined by setting the threshold to 690 mg/cm³. The interassay coefficients of variation for the pQCT measurements were less than 2%.

Histological analyses

For the assessment of dynamic histomorphometric indices, mice were injected with calcein (16 mg/kg body weight) sc at 10 d and 3 d before being killed, after which the left tibiae were excised and fixed with ethanol, and the undecalcified bones were embedded in glycolmethacrylate. Three-micrometer sagittal sections from the proximal parts of tibiae were stained with toluidine blue and were visualized under fluorescent light microscopy for calcein labeling. The specimens were subjected to histomorphometric analyses using a semiautomated system (Osteoplan II; Carl Zeiss, Oberkochen, Germany), and measurements were made at ×400 magnification. Parameters for the trabecular bone were measured in an area 1.2 mm in length, from 250 μm below the growth plate at the proximal metaphysis of the tibiae. Nomenclature, symbols, and units are those recommended by the Nomenclature Committee of the American Society for Bone and Mineral Research (18).

Serum biochemical assays

For serum IGF-I levels, acid ethanol extraction was used to remove the IGF-binding proteins, and the extracted samples were assayed for IGF-I with a RIA kit from Nichols Institute Diagnostics (San Juan Capistrano, CA). Serum osteocalcin levels were determined by using the competitive RIA kit (Biomedical Technologies, Stoughton, MA). The sensitivity of the assay was 19 ng/ml, and the interassay and intraassay coefficients of variation were less than 10%. Serum ALP activity was determined by liquitech ALP kit (Roche Diagnostics, Basel, Switzerland) with an autoanalyzer (type 7170; Hitachi High-Technologies Corporation, Tokyo, Japan). ALP activity of the blood samples was expressed as nanomoles per minute and per milligram of protein.

Statistical analysis

Means of groups were compared by ANOVA, and significance of differences was determined by *post hoc* testing using Bonferroni's method.

FIG. 1. Effects of PTH on cultured osteoblasts isolated from neonatal mouse calvariae. A, IGF-I mRNA level determined by real-time quantitative RT-PCR (left), IGF-I protein level in the culture medium (middle), and ALP activity in the cell lysate (right) in the primary calvarial osteoblast culture in the presence and absence of PTH (100 nM), an antibody against IGF-I (α-IGF-I, 5 nM), and recombinant mouse IGF-I (rmIGF-I, 10 ng/ml) for 2 wk. Data are expressed as means (bars) ± SEM (error bars) for eight wells per group. *, Significant increase compared with the control culture, P < 0.01; #, significant inhibition by α-IGF-I, P < 0.05. B, Protein levels by immunoprecipitation (IP) and immunoblotting (IB) of IGF-I receptor, insulin receptor, IRS-1, and IRS-2 with or without phosphorylation in osteoblasts cultured with PTH (100 nM) for the indicated times. Some of the cell lysates were immunoprecipitated with an antiphosphotyrosine antibody (α-PY), and the cell lysates with or without (−) the immunoprecipitation were immunoblotted with an antimouse IGF-I receptor (α-IGF-IR), an antimouse insulin receptor (α-IR), an antimouse IRS-1 (α-IRS-1), or an antimouse IRS-2 antibody (α-IRS-2). Some of the cell lysates were reciprocally immunoprecipitated with α-IGFR or α-IR and immunoblotted with α-PY. Blottings with an anti-β-actin (α-actin) were used as loading controls. Similar results were obtained in five independent experiments. The graph below shows the mean values of the band intensities of phosphorylated proteins normalized to α-actin quantified using densitometry in five independent experiments. Data are expressed as the ratio of the value at time zero. Although the data of proteins without phosphorylation are not shown in the graph, they were not significantly affected by PTH during the observation period (the ratio values were from 0.8–1.2). Data are expressed as means (bars) ± SEM (error bars) of five independent experiments. *, Significant difference from that at time zero, P < 0.01.
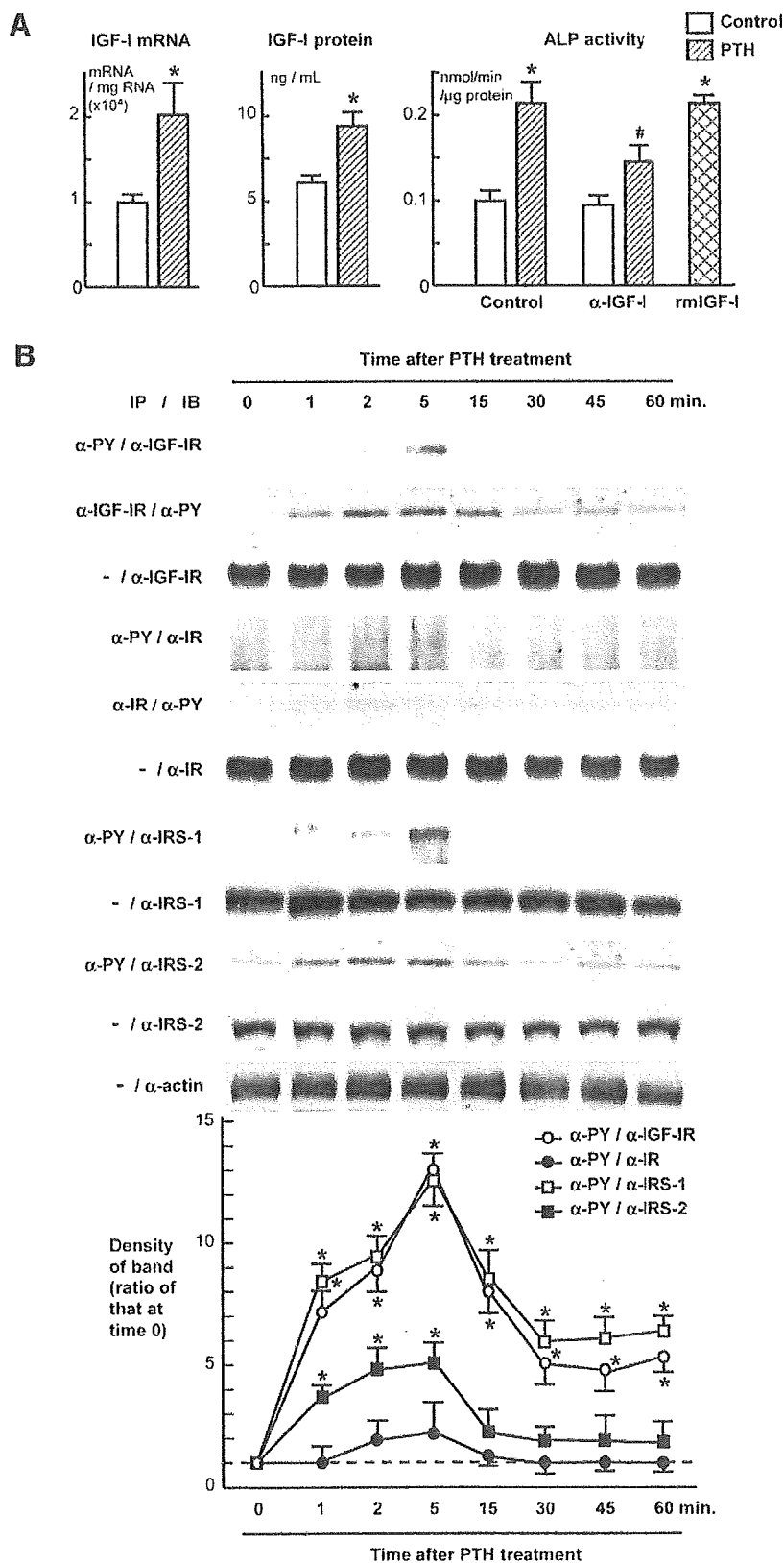
Results

Effects of PTH on cultured osteoblasts

We first examined the effects of recombinant human PTH(1–34) in the cultures of primary osteoblasts derived from mouse calvariae. IGF-I mRNA level determined by real-time RT-PCR, IGF-I protein level in the cultured medium, and ALP activity in the cell lysate were all increased about 2-fold with PTH (100 nM) treatment compared with the control cultures (Fig. 1A). A neutralizing antibody against IGF-I significantly, although not completely, suppressed the PTH stimulation of ALP activity. Furthermore, addition of a recombinant mouse IGF-1 at a concentration similar to that of endogenous IGF-I (10 mg/ml) stimulated by PTH increased the ALP activity to a level similar to that by PTH. These lines of results confirm that the PTH anabolic action is, at least partly, mediated by the IGF-I production in osteoblasts, as previously reported (8, 11, 12).

To provide some insights into signaling pathways that are involved in the PTH action on primary osteoblasts, we examined the phosphorylations of IGF-I receptor, insulin receptor, IRS-1, and IRS-2 in five independent experiments (Fig. 1B). Immunoprecipitation and immunoblotting analyses revealed that phosphorylations of IGF-I receptor and IRS-1 were clearly induced at 1 min and reached maximum at 5 min. IRS-2 was also phosphorylated by PTH, although not as strongly as IGF-I receptor and IRS-1. Insulin receptor was hardly phosphorylated by PTH. None of the protein levels of IGF-I receptor, insulin receptor, IRS-1, or IRS-2 were

altered by PTH during the observation period up to 60 min, suggesting that PTH does not show transcriptional or translational regulation of these signaling molecules. These results indicate that IGF-I production followed by the activation of its intracellular signaling pathways may be related to the PTH action in osteoblasts.

Effects of PTH on bones in IRS-1−/− and IRS-2−/− mice

To learn the roles of the IRS-1 and IRS-2 in the PTH action on bone *in vivo*, we analyzed the PTH effects on the knockout mice by comparing them with those of respective WT littermates using radiological and histological analyses. Both knockout mice were healthy, with no abnormality in major organs except that *IRS-1−/−* mice alone showed about 20% shorter limbs and trunk, whereas *IRS-2−/−* mice were normal in size compared with WT littermates (19–21). The mice (10 wk old, males) were given daily sc injections of PTH (80 μg/kg) or vehicle for 4 wk, after which their femurs, tibiae, and lumbar vertebrae underwent radiological and histological analyses. As we previously reported for bone phenotypes under physiological conditions (16, 17), both knockout mice showed osteopenia when injected with vehicle: BMDs of femur, tibia, and lumbar vertebra in *IRS-1−/−* and those of femur and tibia in *IRS-2−/−* were significantly lower than respective WT littermates (Fig. 2). The PTH injection increased BMDs of these bones 10–20% in WT; however, this increase was hardly seen in the *IRS-1−/−* bones (Fig. 2A). The stimulations by PTH, on the contrary, seen in the *IRS-*
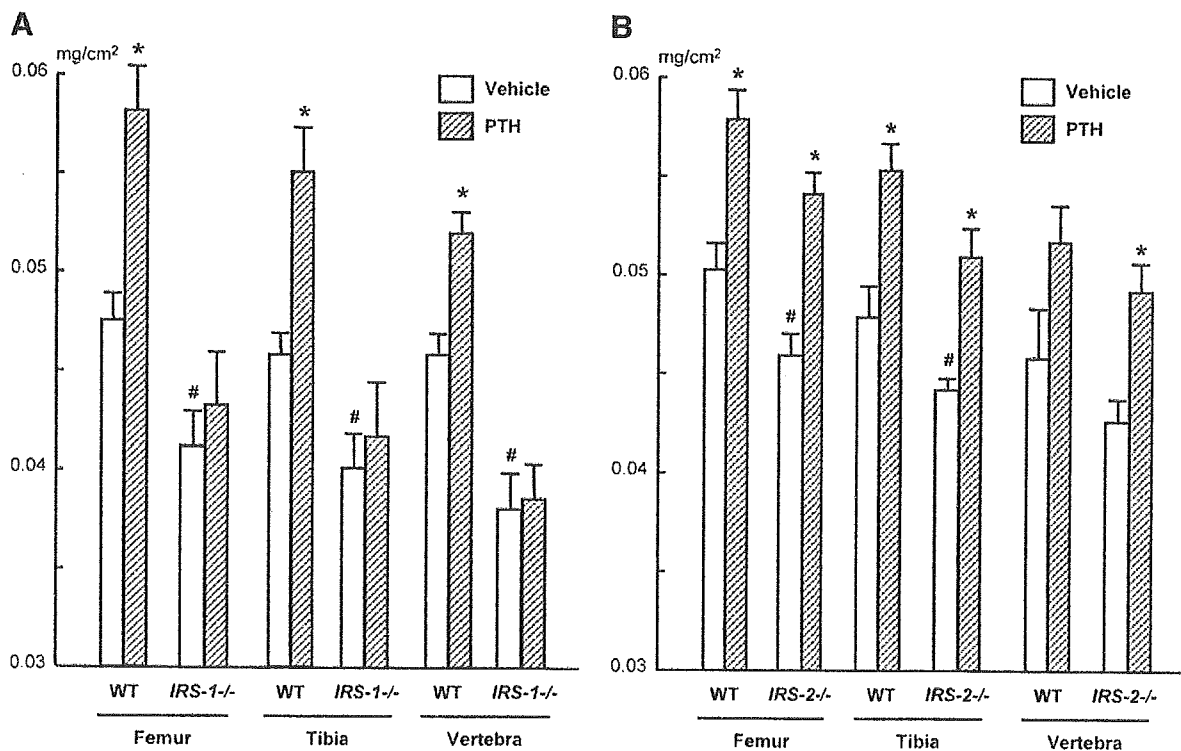

FIG. 2. Effects of PTH treatment on bone densities in *IRS-1−/−* mice (A) and *IRS-2−/−* mice (B), compared with respective WT littermates. *IRS-1−/−* mice and the littermates and *IRS-2−/−* mice and the littermates (males, 10 wk old, n = 10/group) received daily sc injections of either PTH (80 μg/kg body weight) or vehicle for 4 wk. Mice were killed; and the right femurs, tibiae, and L2–L5 vertebral bodies were excised. BMD values of the entire femurs, tibiae, and vertebral bodies were determined using dual-energy x-ray absorptiometry. Data are expressed as means (*bars*) ± SEM (*error bars*) of 10 bones per group. *, Significant effect of PTH, $P < 0.01$; #, significant difference from WT, $P < 0.01$.

2−/− bones were similar to those of the WT littermates (Fig. 2B). These results suggest that IRS-1, but not IRS-2, is needed for the bone anabolic action of PTH.

We further examined trabecular and cortical bones separately in the femurs using pQCT (Fig. 3). In trabecular bones at the distal metaphysis of femurs, both *IRS-1*−/− and *IRS-2*−/− mice showed lower bone density (Fig. 3, A and C). PTH injection increased the trabecular bone density about 60% in WT. Here again, this PTH effect was abolished by the IRS-1 deficiency but was not altered by the IRS-2 deficiency. In the cortical bones at the midshaft of the femurs, although the PTH effects on cortical thickness were milder than those on the trabecular density, this was blocked by the IRS-1 deficiency, although not by the IRS-2 deficiency (Fig. 3, B and D).

Histological features of the proximal tibiae showed decreases of trabecular bones in vehicle-treated *IRS-1*−/− and *IRS-2*−/− mice compared with the respective WT littermates (Fig. 4). After PTH treatment for 4 wk, increases of these bones were observed in *IRS-2*−/− and WT littermates to a similar extent (Fig. 4B), whereas no increase was observed in the *IRS-1*−/− trabeculae (Fig. 4A). Bone histomorphometric measurements in this area confirmed that the PTH injection augmented the bone volume (trabecular bone volume expressed as a percent of total tissue volume) of WT mice by 50–60%, with the increases of both bone formation parameters (percent of bone surface covered by cuboidal osteoclasts, and bone formation rate) and resorption parameters (percent of bone surface covered by mature osteoclasts, and percent of eroded surface), indicating a high bone turnover
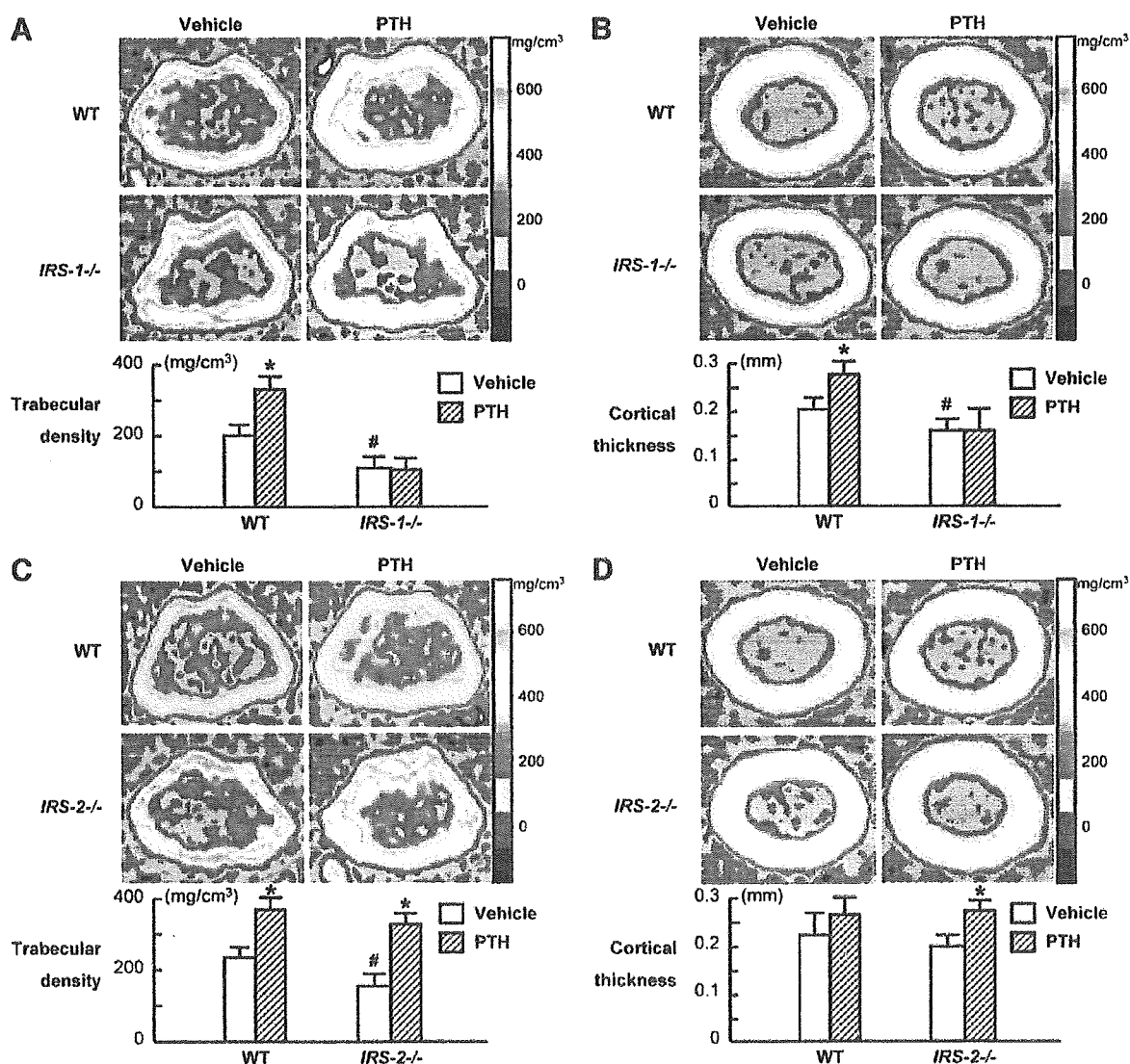

FIG. 3. Effects of PTH treatment on trabecular and cortical bones in *IRS-1*−/− mice (A and B) and *IRS-2*−/− mice (C and D), compared with respective WT littermates. After daily injections of either PTH (80 µg/kg body weight) or vehicle for 4 wk, mice were killed, and the distal metaphysis (A and C) and the middiaphysis (B and D) of the excised left femurs underwent pQCT analysis. The color gradient indicating bone density is shown in the *right bars*. The trabecular density at the metaphysis and the cortical thickness at the middiaphysis are shown in the graphs *below*. Data in all graphs are expressed as means (*bars*) ± SEMs (*error bars*) of 10 bones per group. *, Significant effect of PTH, $P < 0.01$; #, significant difference from WT, $P < 0.01$.
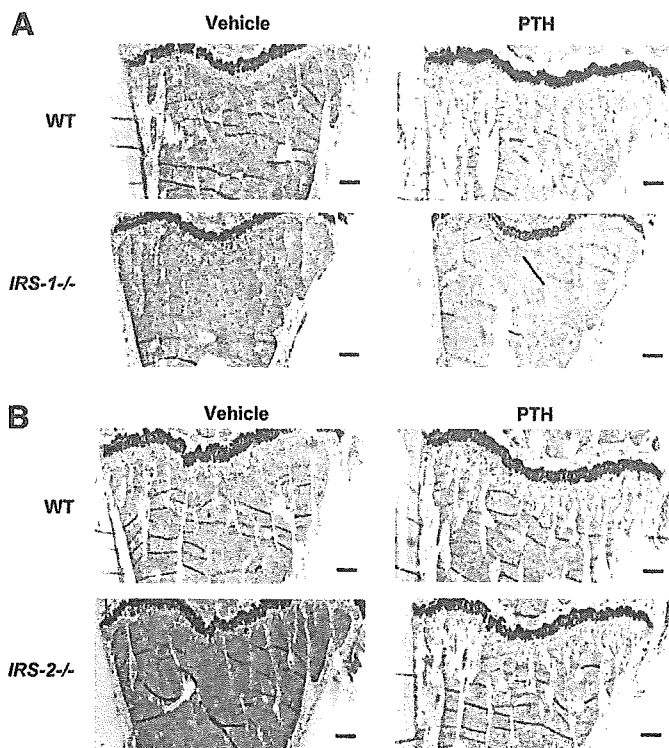
A

B

FIG. 4. Effects of PTH treatment on histological features of the proximal metaphysis of tibiae in *IRS-1−/−* mice (A) and *IRS-2−/−* mice (B), compared with respective WT littermates. After death, the left tibiae were excised, fixed, and embedded in GMA without decalcification, and the sagittal sections were stained by toluidine blue. Representative samples are shown from mice of each genotype given either PTH or vehicle. Data of histomorphometric analyses are shown in Table 1. *Bar*, 100 μm.

state (Table 1). *IRS-1−/−* and *IRS-2−/−* mice showed 30–40% lower bone volume than respective WT littermates when injected with vehicle. As we previously reported (16, 17), *IRS-1−/−* exhibited a low bone turnover, with decreases in both bone formation and resorption parameters, whereas *IRS-2−/−* mice showed an uncoupling status of bone turnover, with decreased bone formation and increased bone resorption. The PTH injection affected neither the bone volume nor the bone turnover in the *IRS-1−/−* mice; however, in the *IRS-2−/−* mice, PTH increased bone volume mainly

through the up-regulation of bone formation rather than bone resorption.

Effects of PTH on blood chemistries in IRS-1−/− and IRS-2−/− mice

The serum markers osteocalcin and ALP supported the increase of bone formation by the PTH injection in WT mice (Fig. 5). Here again, these stimulations were not seen in *IRS-1−/−* mice but were maintained in *IRS-2−/−* mice. Because the serum IGF-I levels were not different between PTH- and vehicle-treated mice in all genotypes, IGF-I that is induced by PTH, as shown in Fig. 1A, seemed not to act as a systemic factor but to act locally in bone as an autocrine/paracrine factor.

Discussion

The present study demonstrated that the bone anabolic function of PTH is mediated by the activation of IGF-1R and IRS-1, but not IRS-2, as a downstream signaling of IGF-I that acts locally in bone. Although IRS-1 and IRS-2 are known to be essential for intracellular signaling of IGF-I and insulin, these two adaptor molecules have distinct biological roles and are differentially expressed in a variety of cells. Regarding glucose homeostasis, IRS-1 plays an important role in the metabolic actions of insulin, mainly in skeletal muscle and adipose tissue, whereas IRS-2 does so in the liver (22). Our previous studies revealed that only IRS-1, but not IRS-2, was expressed in the cartilage of the growth plate or the fracture callus, so that skeletal growth and fracture healing were impaired in *IRS-1−/−* mice, whereas they were normal in *IRS-2−/−* mice (21, 23). In bone, IRS-1 is expressed solely in cells of osteoblast lineage, whereas IRS-2 is expressed in cells of both osteoblast and osteoclast lineages (16, 17). As described above, our previous studies on bones of these two knockout mice disclosed that IRS-1 is important for maintaining bone turnover, and IRS-2 for maintaining predominance of anabolic function over catabolic function of osteoblasts (16, 17). In the meantime, previous and present studies have shown that PTH treatment increases bone turnover in animals and humans (24, 25). The fact that the suppression of bone turnover by IRS-1 deficiency suppressed the bone anabolic action of PTH suggests the importance of elevated turnover for the PTH function. This is consistent with the

TABLE 1. Histomorphometry of trabecular bones in proximal tibiae

	BV/TV (%)	Ob.S/BS (%)	BFR (mm³/cm²/year)	Oc.S/BS (%)	ES/BS (%)
WT + vehicle	9.35 ± 0.69	8.38 ± 0.80	4.96 ± 0.62	5.28 ± 1.39	6.02 ± 0.99
WT + PTH	14.23 ± 1.84[a]	12.27 ± 1.89	8.21 ± 0.83[a]	10.51 ± 1.35[a]	9.14 ± 0.51[a]
IRS-1−/− + vehicle	5.97 ± 0.62[b]	2.67 ± 1.02[b]	1.06 ± 0.29[b]	2.23 ± 0.38[b]	3.42 ± 0.59[b]
IRS-1−/− + PTH	6.25 ± 0.73	4.50 ± 0.93	1.31 ± 0.38	2.71 ± 1.03	4.14 ± 1.22
WT + vehicle	9.94 ± 0.81	8.49 ± 1.53	4.22 ± 0.29	4.90 ± 0.78	5.35 ± 0.71
WT + PTH	15.79 ± 1.60[a]	13.61 ± 2.24	9.72 ± 1.83[a]	8.84 ± 1.27[a]	9.60 ± 1.21[a]
IRS-2−/− + vehicle	6.86 ± 0.63[b]	12.93 ± 2.83	2.06 ± 0.31[b]	7.92 ± 0.69[b]	9.22 ± 1.09[b]
IRS-2−/− + PTH	16.95 ± 2.27[a]	15.71 ± 1.80	8.71 ± 0.59[a]	9.93 ± 1.43	11.42 ± 2.01

Parameters for the trabecular bone were measured in an area 1.2 mm in length from 250 μm below the growth plate at the proximal metaphysis of the tibiae in Villanueva-Goldner and calcein double-labeled sections. Data expressed as means and SEM for 10 bones per group. BV/TV, Trabecular bone volume expressed as a percentage of total tissue volume; Ob.S/BS, percentage of bone surface covered by cuboidal osteoblasts; BFR, bone formation rate; Oc.S/BS, percentage of bone surface covered by mature osteoclasts; ES/BS, percentage of eroded surface.
[a] Significant effect of PTH, *P* < 0.01.
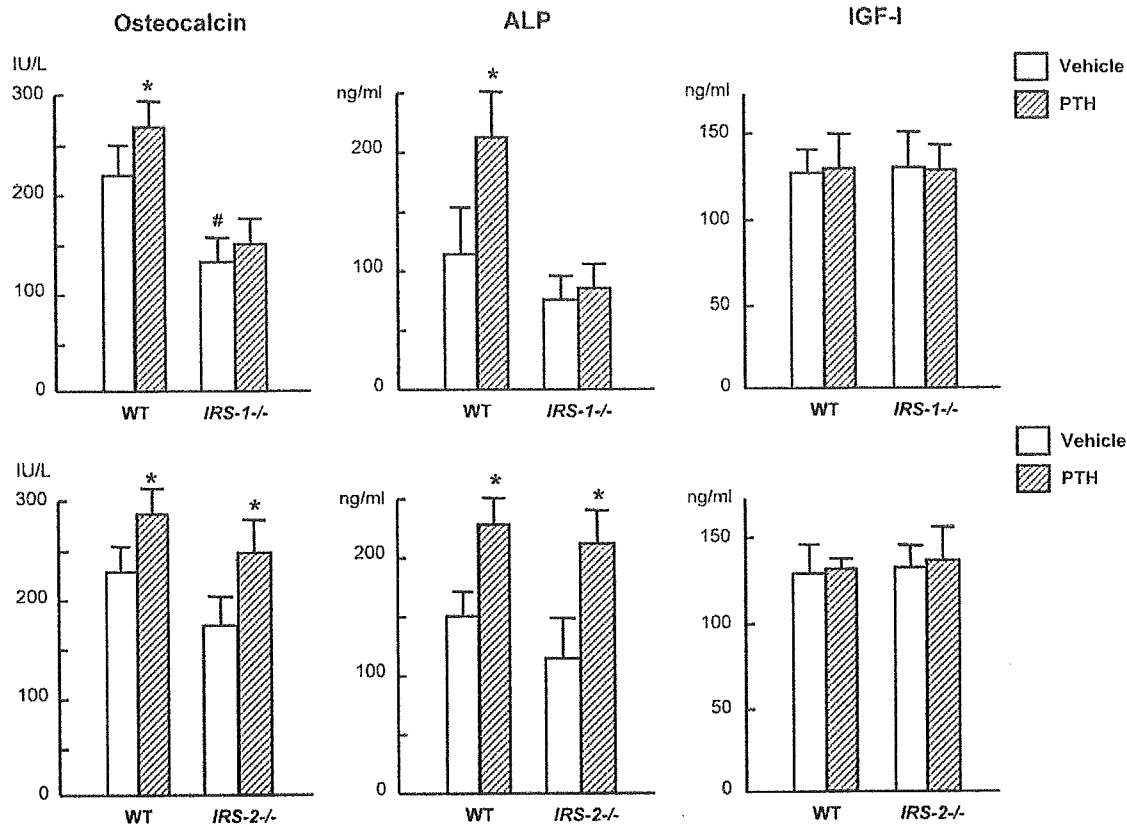[b] Significant difference from WT, *P* < 0.01.

FIG. 5. Effects of PTH treatment on serum osteocalcin, ALP, and IGF-I levels in IRS-1−/− mice and IRS-2−/− mice, compared with respective WT littermates. Mice received either PTH or vehicle for 4 wk as described above, and blood samples were collected by heart puncture before death. The levels were measured as described in *Materials and Methods*. *, Significant effect of PTH, $P < 0.05$; #, significant difference from WT, $P < 0.05$.

results of clinical studies showing that the concurrent use of alendronate, a potent bisphosphonate that markedly suppresses bone turnover, reduced the bone anabolic action of PTH in male and female osteoporosis patients (26, 27).

Because it is unlikely that PTH directly activates IGF-I receptor and IRS-1, there seem to be two possible molecular mechanisms underlying the suppression of PTH action by the IRS-1 deficiency: 1) PTH induces IGF-I production, causing IGF-I receptor and IRS-1 activation; and 2) IRS-1 signaling affects the intracellular signaling lying downstream of the PTH/PTH-related protein receptor after PTH binds to it. The quick phosphorylation of IGF-I receptor and IRS-1 after PTH treatment in primary osteoblast culture in the present study (Fig. 1B) supports the former mechanism. Hormones like PTH and prostaglandin E_2 that increase cAMP synthesis and PKA activation are reported to induce the transcription of IGF-I by way of a C/EBP (CCAAT/enhancer-binding protein)-sensitive element in exon 1 of the IGF-I gene (28, 29). However, the latter possibility cannot be denied, because the inhibition of the PTH stimulation on ALP activity by a neutralizing antibody against IGF-I was not complete, but partial, in the primary osteoblast culture (Fig. 1A). In fact, IRS-1 and PTH/PPR (PTH/PTH-related protein receptor) are known to share several common signaling pathways. The main pathways lying downstream of IRS-1 are PI3K/Akt and MAPKs, which are important regulators of cell growth and differentiation. PTH has been shown to directly activate the

p42/p44 MAPK by protein kinase C-dependent, but Ras-independent, signaling in rat osteoblasts (30) and to up-regulate PI3K/Akt activity, which contributes to the MAPK activation in rat enterocytes (31). In addition, both PTH and IGF-I have been shown to be involved in the activation of c-*fos* expression (32, 33) and cyclin-dependent kinase expression in osteoblasts (34, 35). These lines of evidence indicate the PTH signaling pathway may possibly be affected by the IRS-1 signaling at several points, and the absence of an IRS-1 signaling pathway may result in the failure of PTH to stimulate key target molecules necessary for its anabolic action.

Another potential explanation for the lack of PTH response in IRS-1−/− mice could be the impairment of proliferation or differentiation ability of osteoprogenitor cells, so that they are insensitive not only to PTH but also to other stimulations. In fact, our present and previous studies demonstrated the decreases in histomorphometric parameters and serum markers for bone formation in IRS-1−/− mice under physiological conditions (16). In this regard, however, our previous study has shown that proliferation and differentiation of primary calvarial cells were stimulated, responding to fibroblast growth factor-2 and bone morphogenetic protein-2, respectively, similarly to those of the WT cells, indicating that functions of IRS-1−/− cells are normal as long as adequate signals other than IGF-I signal were applied (16). Hence, the decreased bone formation under physiological conditions in IRS-1−/− mice is likely to be due to the deficit

of anabolic signaling of endogenous IGF-I. Interestingly, PTH increased the IGF-I protein level in the culture medium of primary osteoblasts (Fig. 1A) but did not affect the serum IGF-I level *in vivo* (Fig. 5), indicating the importance of local action of IGF-I as an autocrine/paracrine factor for bone formation rather than its systemic action as a hormone. This result is consistent with previous reports that disruption of IGF-I genes, specifically in liver, decreased serum IGF-I by 80% but caused no skeletal abnormality (36, 37). Because the remaining 20% IGF-I in serum is probably derived from several tissues, including bone, it is not surprising that PTH treatment did not increase circulating levels of IGF-I. The findings that PTH anabolic effects can be suppressed by an IGF-I-neutralizing antibody in osteoblast cultures in the present and previous studies (11, 12) also support the idea that the PTH-induced bone formation involves increased local production, but not increased circulating levels, of IGF-I.

The requirement of IGF-I/IRS-1 for mediating the anabolic effects of bone regulatory hormones may not be unique to PTH, because previous findings have revealed that many of the major hormones exert significant effects on IGF-I expression. GH is a well-known stimulus of IGF-I production in a variety of tissues, including bone, and exerts its effects on bone mainly through IGF-I mediation (38). Estradiol, another important regulator of skeletal metabolism, has been shown to increase IGF-I production, and IGF-I receptor-blocking antibodies inhibited the proliferative effect of estradiol in rat osteoblasts (39, 40). Similarly, other hormones with potent effects on bone, such as thyroid hormone and androgens, alter IGF-I levels in bone in a manner consistent with IGF-I playing a role in the actions of these hormones on bone (41, 42). Although these studies did not examine the involvement of IRS-1 or IRS-2 in their anabolic actions, it is possible that the IGF/IRS pathway might be a common signaling for actions of these major hormones in bone. Further understanding of the molecular mechanism by which the hormones induce IGF-I and the intracellular signaling that lies downstream of IGF-I/IRS in osteoblasts will greatly help to elucidate the complex network of bone formation under systemic regulations.

Acknowledgments

References

1. **Dempster DW, Cosman F, Parisien M, Shen V, Lindsay R** 1994 Anabolic actions of parathyroid hormone on bone. Endocr Rev 15:261–280
2. **Eastell R** 1998 Treatment of postmenopausal osteoporosis. N Engl J Med 338:736–745
3. **Neer RM, Arnaud CD, Zanchetta JR, Prince R, Gaich GA, Reginster JY, Hodsman AB, Eriksen EF, Ish-Shalom S, Genant HK, Wang O, Mitlak BH** 2001 Effect of parathyroid hormone (1–34) on fractures and bone mineral density in postmenopausal women with osteoporosis. N Engl J Med 344:1434–1441
4. **Rosen CJ** 2003 The cellular and clinical parameters of anabolic therapy for osteoporosis. Crit Rev Eukaryot Gene Expr 13:25–38
5. **Isogai Y, Akatsu T, Ishizuka T, Yamaguchi A, Hori M, Takahashi N, Suda T** 1996 Parathyroid hormone regulates osteoblast differentiation positively or negatively depending on the differentiation stages. J Bone Miner Res 11:1384–1393
6. **Nishida S, Yamaguchi A, Tanizawa T, Endo N, Mashiba T, Uchiyama Y, Suda T, Yoshiki S, Takahashi E** 1994 Increased bone formation by intermittent parathyroid hormone administration is due to the stimulation of proliferation and differentiation of osteoprogenitor cells in bone marrow. Bone 15:717–723
7. **Jilka RL, Weinstein RS, Bellido T, Roberson P, Parfitt AM, Manolagas SC** 1999 Increased bone formation by prevention of osteoblast apoptosis with parathyroid hormone. J Clin Invest 104:439–446
8. **McCarthy TL, Centrella M, Canalis E** 1989 Parathyroid hormone enhances the transcript and polypeptide levels of insulin-like growth factor I in osteoblast-enriched cultures from fetal rat bone. Endocrinology 124:1247–1253
9. **Watson P, Lazowski D, Han V, Fraher L, Steer B, Hodsman A** 1995 Parathyroid hormone restores bone mass and enhances osteoblast insulin-like growth factor I gene expression in ovariectomized rats. Bone 16:357–365
10. **Canalis E** 1993 Insulin like growth factors and the local regulation of bone formation. Bone 14:273–276
11. **Canalis E, Centrella M, Burch W, McCarthy TL** 1989 Insulin-like growth factor I mediates selective anabolic effects of parathyroid hormone in bone cultures. J Clin Invest 83:60–65
12. **Ishizuya T, Yokose S, Hori M, Noda T, Suda T, Yoshiki S, Yamaguchi A** 1997 Parathyroid hormone exerts disparate effects on osteoblast differentiation depending on exposure time in rat osteoblastic cells. J Clin Invest 99:2961–2970
13. **Miyakoshi N, Kasukawa Y, Linkhart TA, Baylink DJ, Mohan S** 2001 Evidence that anabolic effects of PTH on bone require IGF-I in growing mice. Endocrinology 142:4349–4356
14. **Bikle DD, Sakata T, Leary C, Elalieh H, Ginzinger D, Rosen CJ, Beamer W, Majumdar S, Halloran BP** 2002 Insulin-like growth factor I is required for the anabolic actions of parathyroid hormone on mouse bone. J Bone Miner Res 17:1570–1578
15. **Kadowaki T, Tobe K, Honda-Yamamoto R, Tamemoto H, Kaburagi Y, Momomura K, Ueki K, Takahashi Y, Yamauchi T, Akanuma Y, Yazaki Y** 1996 Signal transduction mechanism of insulin and insulin-like growth factor-1. Endocr J 43:S33–S41
16. **Ogata N, Chikazu D, Kubota N, Terauchi Y, Tobe T, Azuma Y, Ohta T, Kadowaki T, Nakamura K, Kawaguchi H** 2000 Insulin receptor substrate-1 in osteoblast is indispensable for maintaining bone turnover. J Clin Invest 105:935–943
17. **Akune T, Hoshi K, Kubota Y, Terauchi K, Tobe Y, Azuma T, Ohta T, Nakamura K, Kawaguchi H** 2002 Insulin receptor substrate-2 maintains predominance of anabolic function over catabolic function of osteoblasts. J Cell Biol 159:147–156
18. **Parfitt AM, Drezner MK, Glorieux FH, Kanis JA, Malluche H, Meunier PJ, Ott SM, Recker RR** 1987 Bone histomorphometry: standardization of nomenclature, symbols, and units. Report of the ASBMR Histomorphometry Nomenclature Committee. J Bone Miner Res 2:595–610
19. **Tamemoto H, Kadowaki T, Tobe K, Yagi T, Sakura H, Hayakawa T, Terauchi Y, Ueki K, Kaburagi Y, Satoh S, Nagai R, Yazaki T** 1994 Insulin resistance and growth retardation in mice lacking insulin receptor substrate-1. Nature 372:182–186
20. **Kubota N, Tobe K, Terauchi Y, Eto K, Yamauchi T, Suzuki R, Tsubamoto Y, Komeda K, Nakano R, Miki H, Satoh S, Sekihara H, Sciacchitano S, Lesniak M, Aizawa S, Nagai R, Kimura S, Akanuma Y, Taylor SI, Kadowaki T** 2000 Disruption of insulin receptor substrate 2 causes type 2 diabetes because of liver insulin resistance and lack of compensatory β-cell hyperplasia. Diabetes 49:1880–1889
21. **Hoshi K, Ogata N, Shimoaka T, Terauchi Y, Kadowaki T, Kenmotsu S, Chung UI, Ozawa H, Nakamura K, Kawaguchi H** 2004 Deficiency of insulin receptor substrate-1 impairs skeletal growth through early closure of epiphyseal cartilage. J Bone Miner Res 19:214–223
22. **Bruning JC, Winnay J, Cheatham B, Kahn CR** 1997 Differential signaling by insulin receptor substrate 1 (IRS-1) and IRS-2 in IRS-1-deficient cells. Mol Cell Biol 17:1513–1521
23. **Shimoaka T, Kamekura S, Chikuda H, Hoshi K, Chung UI, Akune T, Maruyama Z, Komori T, Matsumoto M, Ogawa W, Terauchi Y, Kadowaki T, Nakamura K, Kawaguchi H** 2004 Impairment of bone healing by insulin receptor substrate-1 deficiency. J Biol Chem 279:15314–15322
24. **Sato M, Westmore M, Ma YL, Schmidt A, Zeng QQ, Glass EV, Vahle J, Brommage R, Jerome CP, Turner CH** 2004 Teriparatide [PTH(1–34)] strengthens the proximal femur of ovariectomized nonhuman primates despite increasing porosity. J Bone Miner Res 19:623–629
25. **Dempster DW, Cosman F, Kurland ES, Zhou H, Nieves J, Woelfert L, Shane E, Plavetic K, Muller R, Bilezikian J, Lindsay R** 2001 Effects of daily treatment with parathyroid hormone on bone microarchitecture and turnover in patients with osteoporosis: a paired biopsy study. J Bone Miner Res 16:1846–1853
26. **Black DM, Greenspan SL, Ensrud KE, Palermo L, McGowan JA, Lang TF, Garnero P, Bouxsein ML, Bilezikian JP, Rosen CJ; PTH Study Investigators**

2003 The effects of parathyroid hormone and alendronate alone or in combination in postmenopausal osteoporosis. N Engl J Med 349:1207–1215

27. Finkelstein JS, Hayes A, Hunzelman JL, Wyland JJ, Lee H, Neer RM 2003 The effects of parathyroid hormone, alendronate, or both in men with osteoporosis. N Engl J Med 349:1216–1226

28. Umayahara Y, Billiard J, Ji C, Centrella M, McCarthy TL, Rotwein P 1999 CCAAT/enhancer-binding protein δ is a critical regulator of insulin-like growth factor-I gene transcription in osteoblasts. J Biol Chem 274:10609–10617

29. Chang W, Rewari A, Centrella M, McCarthy TL 2004 Fos-related antigen 2 controls protein kinase A-induced CCAAT/enhancer-binding protein β expression in osteoblasts. J Biol Chem 279:42438–42444

30. Swarthout JT, Doggett TA, Lemker JL, Partridge NC 2001 Stimulation of extracellular signal-regulated kinases and proliferation in rat osteoblastic cells by parathyroid hormone is protein kinase C-dependent. J Biol Chem 276:7586–7592

31. Gentili C, Morelli S, Russo De Boland A 2002 Involvement of PI3-kinase and its association with c-Src in PTH-stimulated rat enterocytes. J Cell Biochem 86:773–783

32. Lee K, Deeds JD, Chiba S, Un-No M, Bond AT, Segre GV 1994 Parathyroid hormone induces sequential c-fos expression in bone cells in vivo: in situ localization of its receptor and c-fos messenger ribonucleic acids. Endocrinology 134:441–450

33. Merriman HL, La Tour D, Linkhart TA, Mohan S, Baylink DJ, Strong DD 1990 Insulin-like growth factor-I and insulin-like growth factor-II induce c-fos in mouse osteoblastic cells. Calcif Tissue Int 46:258–262

34. Onishi T, Zhang W, Cao X, Hruska K 1997 The mitogenic effect of parathyroid hormone is associated with E2F-dependent activation of cyclin-dependent kinase 1 (cdc2) in osteoblast precursors. J Bone Miner Res 12:1596–1605

35. Furlanetto RW, Harwell SE, Frick KK 1994 Insulin-like growth factor-I induces cyclin-D1 expression in MG63 human osteosarcoma cells in vitro. Mol Endocrinol 8:510–517

36. Yakar S, Liu JL, Stannard B 1999 Normal growth and development in the absence of hepatic insulin-like growth factor I. Proc Natl Acad Sci USA 96:7324–7329

37. Sjogren K, Liu JL, Blad K 1999 Liver-derived insulin-like growth factor I (IGF-I) is the principal source of IGF-I in blood but is not required for postnatal body growth in mice. Proc Natl Acad Sci USA 96:7088–7092

38. Ohlsson C, Bengtsson BA, Isaksson OG, Andreassen TT, Slootweg MC 1998 Growth hormone and bone. Endocr Rev 19:55–79

39. Gray TK, Mohan S, Linkhart TA, Baylink DJ 1989 Estradiol stimulates in vitro the secretion of insulin-like growth factors by the clonal osteoblastic cell line, UMR106. Biochem Biophys Res Commun 158:407–412

40. Cheng M, Zaman G, Rawlinson SC, Mohan S, Baylink DJ, Lanyon LE 1999 Mechanical strain stimulates ROS cell proliferation through IGF-II and estrogen through IGF-I. J Bone Miner Res 14:1742–1750

41. Gori F, Hofbauer LC, Conover CA, Khosla S 1999 Effects of androgens on the insulin-like growth factor system in an androgen-responsive human osteoblastic cell line. Endocrinology 140:5579–5586

42. Huang BK, Golden LA, Tarjan G, Madison LD, Stern PH 2000 Insulin-like growth factor I production is essential for anabolic effects of thyroid hormone in osteoblasts. J Bone Miner Res 15:188–197

Endocrinology is published monthly by The Endocrine Society (http://www.endo-society.org), the foremost professional society serving the endocrine community.